Tartu Ülikool
Loodus- ja täppisteaduste valdkond
Ökoloogia ja maateaduste instituut
Geoloogia osakond

Magistritöö geoloogias (30EAP)

Raman spectroscopy study of the sedimentary organic material thermal alteration in the Paleoproterozoic Francevillian Basin, Gabon

Orgaanilise ainese muutumisastme kaardistamine Raman spektroskoopiaga Paleoproterosoilistes Franceville'i basseini setendites, Gabon

Georg Rahu

juhendajad: Kalle Kirsimäe,
Tavo Romann

Tartu 2025

Raman spectroscopy study of the sedimentary organic material thermal alteration in the Paleoproterozoic Francevillian Basin, Gabon

The aim of this master's thesis was to discern the lateral and stratigraphic variability of thermal alteration in organic material and pyrobitumen (solidified petroleum) of the Franceville, Lastoursville and Okondja sub-basins of the Francevillian basin using Raman spectroscopy and reconstruct the extent of thermal overprint on preserved sedimentary organic material by diagenesis-metamorphism, later fluids and magmatism.

Studied material was sampled from both drillcores and outcrops from the Franceville, Lastoursville and Okondja sub-basins. Spatial variation in temperature between the three sub-basins was detected with Franceville and Okondja having similar temperatures and Lastoursville having lower temperatures, though still over the threshold for biomarker preservation.

Keywords: Raman spectroscopy, geothermometry, organic material

CERCS: P420 Petrology, mineralogy, geochemistry

Orgaanilise aines muutumisasme kaardistamine Raman spektroskoopiaga Paleoproterosoilistes Franceville basseini setendites, Gabon

Käesoleva magistritöö eesmärk oli Raman spektroskoopia abil uurida Franceville'i basseini Franceville'i, Lastoursville'i ja Okondja alambasseinide orgaanilise aine ja pürobituumeni (tahkestunud nafta) termilise muutumise lateraalset ja stratigraafilist varieeruvust ning rekonstrueerida säilinud orgaanilise aine muutust diageneesi, moonde, hilisemate fluidide ja magmatismi mõjudel.

Uuritav materjal koguti Franceville'i, Lastoursville'i ja Okondja alam-basseinide puursüdamikest ja paljanditest. Tulemused viitavad termilise muutuse ruumilisele varieeruvusele. Franceville'i ja Okondja alambasseinides esinevad sarnased temperatuurid ja Lastoursville'i alambasseinis on tempetatuurid oluliselt madalamad, kuid siiski liiga kõrged biomarkerite säilimiseks.

Märksõnad: Raman spektroskoopia, geotermomeetria, orgaaniline aine

CERCS: P420 Petrology, mineralogy, geochemistry

Table of Contents

1. Introduction

The Great Oxidation Event (GOE) represents the most fundamental change ever to Earth's surface environments, the first time when free O_2 began accumulating in the atmosphere (Bekker & Holland, 2012; Holland, 2006; Lyons et al., 2014). This event occurred between 2502 - 2460 million years ago (Ma; Bekker et al., 2020; Gumsley et al., 2017; Warke et al., 2020) and marked an irreversible trajectory from an anoxic to oxic state in the Earth's history. The GOE triggered an avalanche of environmental disturbances and fundamentally reset element cycling modes. However, the exact mechanisms of these changes remain a matter of discussion (e.g., Poulton et al., 2021; Rasmussen et al., 2023; Robbins et al., 2023; Wogan et al., 2022).

Of all the hallmark features that characterise this time in Earth's history, the most-debated phenomenon following the GOE is the Lomagundi-Jatuli Excursion (LJE) – the largest and longest disturbance of the carbon cycle in Earth's history (Hodgskiss & Sperling, 2022; Karhu & Holland, 1996; Melezhik et al., 2007). For 4 billion years, marine carbonate carbon isotope ratios (δ^{13}Ccarb) mostly oscillated around 0 ± 4‰, reflecting a dynamic balance and stability between the major sources and sinks of carbon (Laakso & Schrag, 2022; Schidlowski et al., 1983; Shields & Veizer, 2002; Strauss & Beukes, 1996). In contrast, between 2300 and 2050 Ma (Martin et al., 2013), the LJE shows persistently positive $\delta^{13}C_{carb}$ values of 5 to 15‰, locally reaching +30‰. Thus, the LJE records a mystifying imbalance between Earth's inorganic and organic carbon pools (Bekker et al., 2003; Hayes et al., 1999; Hayes & Waldbauer, 2006; Kump, 1991; Laakso & Schrag, 2022; Marais et al., 1992; Mason et al., 2017; Planavsky et al., 2012; Schidlowski, 1987).

However, since its discovery more than 50 years ago (Galimov et al., 1968; Schidlowski et al., 1975), the underlining causes and mechanisms behind the LJE have remained unknown. The standard model explaining the LJE invokes a positive feedback loop between nutrient flux and primary production (i.e. increased Corg burial driving O_2 excess). This feedback is postulated to have been initiated by acidic weathering caused by the oxidation of sulfide minerals on Earth's surface following the GOE (Bekker & Holland, 2012), likely amplified by tectonic processes and increased continental weathering rates (Bindeman et al., 2018; Campbell & Allen, 2008).

Surprisingly under-emphasised in these mostly geochemical-focussed models is the consideration of the major biospheric evolutionary changes postulated for this time in Earth's history. When oxygenic photosynthesis evolved remains speculative (Fischer et al., 2016; Lyons et al., 2014;

Ohmoto, 1996; Rasmussen et al., 2023; Ward et al., 2019), but it is now generally accepted that marine planktonic cyanobacteria evolved only towards the end of the Proterozoic. Phylogenomic studies suggest that the earlier Proterozoic was likely dominated by filamentous, mat-forming cyanobacteria living on the floor of water bodies (Blank & Sanchez-Baracaldo, 2010; Sánchez-Baracaldo & Cardona, 2020). This "Biomat World" (Javaux & Lepot, 2018; Sánchez-Baracaldo, 2015) typified Proterozoic microbial ecosystems, in contrast to the Modern where primary production is roughly equally divided between marine planktonic microbial organisms and terrestrial vegetation (Duursma & Boisson, 1994). Further, relaxed molecular clock analyses suggest that photosynthetic cyanobacteria originated in (and were restricted to) freshwater environments by at least 2400 Ga before diversifying into coastal brackish and marine environments (Blank & Sanchez-Baracaldo, 2010; Sánchez-Baracaldo et al., 2017).

However, testing of these hypotheses is complicated because of the absence or limited preservation of microbial fossil materials. In the lack of diagnostic microfossils, fossil lipid hydrocarbons can provide valuable information on past ecologies, biological diversity and environmental conditions (Brocks & Summons, 2003). In fact, most of our knowledge of metabolism and diversity on the early Earth derives from such hydrocarbon biomarkers (Hallmann et al., 2022). Currently, the oldest accepted syngenetic biomarker hydrocarbons derive from the Paleo-/Mesoproterozoic Barney Creek Formation of 1.64 Ga age (Summons & Powell, 1986).

The preservation of biomarker signals is hindered by diagenetic and metamorphic processes. Upon burial of organic material in sediments, diagenetic transformations begin (Brocks & Summons 2003). Main changes in organic material begin with thermocatalytic reactions at temperatures around 60 – 70 °C (corresponding to burial to depths of 1.5 – 2 km under stable geothermal conditions), where long kerogen molecules disassemble into shorter chains of carbon. This is also the onset of the formation of oil and gas, where volatile components (H and O) escape and organic material becomes enriched in carbon. Along with alterations in chemical compositions, the carbon structure also begins to organise and finally turns to graphite. The metamorphic grade of organic material in relation to temperature can be measured by chemical composition (H:C ratio, presence of biomarkers) and level of organization of carbon structure (Brocks & Summons 2003).

Because of these processes the likelihood is that most of the Archean and/or Paleoproterozoic rocks are too strongly thermally overprinted at temperatures >200 °C to preserve such signatures (French

et al., 2015). Therefore, it is important to test how much earlier than 1.64 Ga, the currently oldest records (Summons & Powell 1986), we can find the preserved biomarker record to understand the nature of early ecosystems, particularly in the Paleoproterozoic, when oxygen levels started to increase.

Paleoproterozoic successions of the Francevillian Basin in Gabon are unique amongst all known Paleoproterozoic sedimentary sequences by quality of their preservation, having experienced only late diagenetic to very low-grade metamorphic conditions while all other Paleoproterozoic successions have been modified by greenschist-facies and higher metamorphism. Earlier thermal alteration indicators show that the maximum post-depositional temperatures for the Francevillian strata were mostly between 150 – 250 °C, only locally exceeding 300 °C (Lecomte et al., 2020; Lekele Baghekema et al., 2017; Mossman et al., 2001; Ossa Ossa et al., 2013). Also, deformation in the basin is minimal, and most strata are flat-lying to moderately inclined in broad open folds (Weber, 1968).

This suggests that in the Francevillan Basin, organic-rich sediments that might not have been heated to temperatures over 200 – 250 °C, critical for the preservation of the biomarkers and raises the possibility of determining the ecology and biodiversity of the microbial communities of that time, can be found.

The aim of this thesis is to discern the lateral and stratigraphic variability of thermal alteration in organic material and pyrobitumen (solidified petroleum) of the Franceville, Lastoursville and Okondja sub-basins of the Francevillian basin using Raman spectroscopy and reconstruct the extent of thermal overprint on preserved sedimentary organic material by diagenesis-metamorphis, later fluids and magmatism.

2. Geological setting

The Francevillian basin is a Palaeoproterozoic sedimentary intracratonic basin that spans across 42 000 km^2 (Weber & Gauthier-Lafaye 2013) of central and eastern Gabon with thicknesses of 1 – 4 km (Bankole et al., 2015; Gauthier-Lafaye & Weber 1989; Ossa Ossa et al., 2014). It is divided into the Franceville, Okondja, Lastoursville and Booué sub-basins (Figure 1). The volcanoclastic-sedimentary series lies unconformably on the Archean granitoid-greenstone basement and limited by granitic rocks of the North-Gabon domain to the north and by metamorphic rocks of the Chaillu domain to the south. In the west the basin borders the Ogooué orogenic belt, and in the east younger Mesozoic-Cenozoic continental sediments. The basin opened as a rift basin after the doming of migmatites around 2.4 Ga followed by the inversion of the rift basin and the coeval onset of the Eburnean orogeny about 2.2 Ga, and later formation of a pull-apart basin along massive N – S oriented sinistral strike-slip faults (Weber & Gauthier-Lafaye 2013).

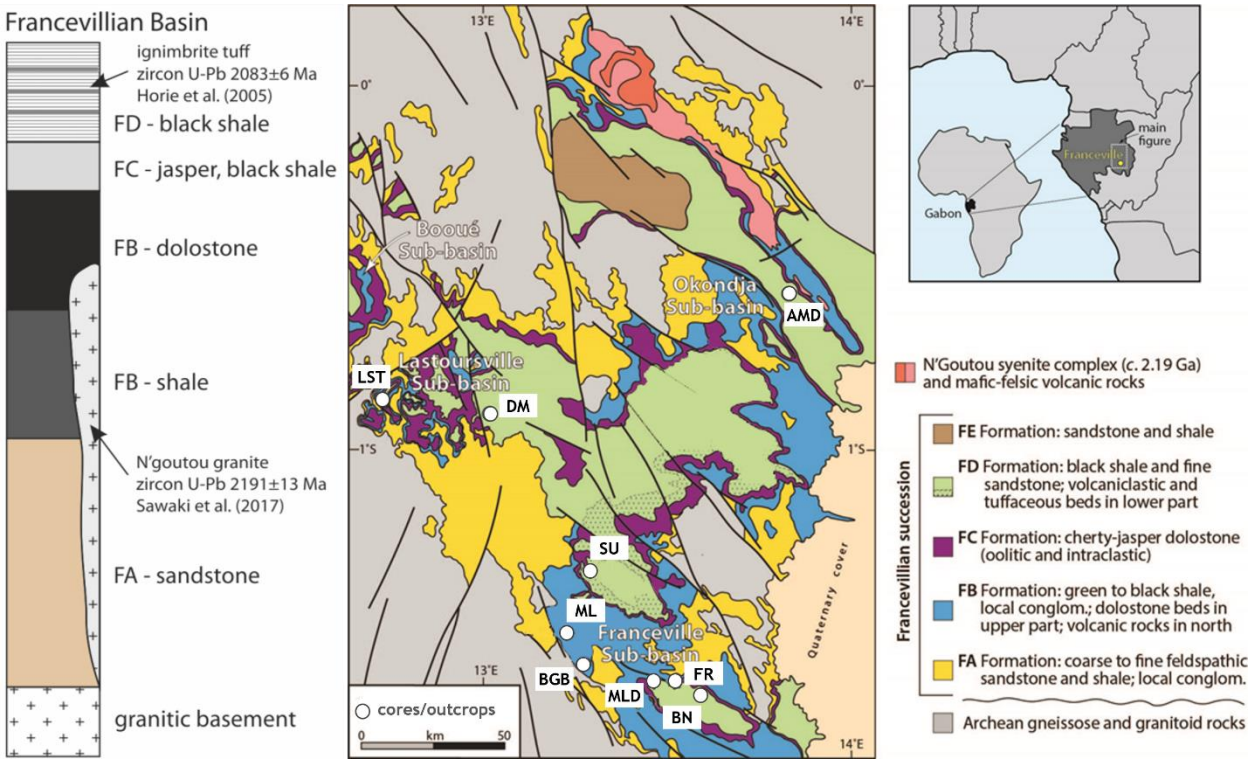

Figure 1. General stratigraphy and geological map of the Francevillian Basin, and location of the studied cores-outcrops AMD – Ambinda; BGB – Bangombé; BN – Biniomi; DM – Doumé; FR – Franceville; LST – LST12; ML – ML594/605; MLD – Moulendé; SU – Sully. Modified after Mayika et al., (2020). Schematic geological map figure of the Francevillian Basin by A. Prave.

The basin fill of the Francevillian has been divided lithostratigraphically into the FA, FB, FC, FD and FE formations (Figure 1, 2). The FA formation consists of fluvial coarse quartz-arenite sandstones and conglomerates followed by tidal sandstones (Bankole et al., 2015; Gauthier-Lafaye & Weber 1989; Lecomte et al., 2020; Ossa Ossa et al., 2014). The thickness of the unit increases from 100 m at the edges to 1000 m towards the center of the basin. Sedimentological structures indicate a general flow direction of west to east (Weber et al., 2016). The upper part of the FA formation hosts the Francevillian uranium deposits and natural nuclear fission reactors (Weber & Gauthier-Lafaye 2013). FA formation also acts as a reservoir rock and hosts pyrobitumen (solidified petroleum) the emplacement of which is associated with U mineralization (Lecomte et al., 2020.

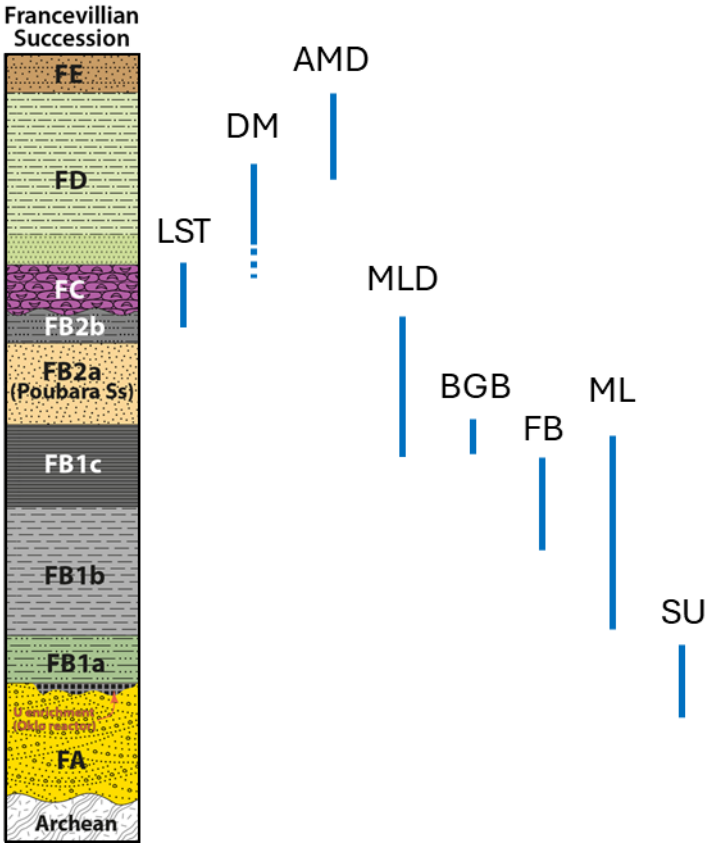

Figure 2. Tentative stratigraphic coverage of the studied drillcores. LST – LST12, DM – Doumé, AMD – Ambinda, SU – Sully, ML – ML593/605, BGB – Bangombé, MLD – Moulendé. Column figure by A. Prave.

The 400 to 1000 m thick Francevillian B formation is divided into two members - the FB1 and FB2. FB1 consists of black shales, calcareous fine grained sediments rich in organic matter interstratified with sandstones and dolomites, indicating episodes of transgression and regression (Bankole et al., 2015; Gauthier-Lafaye & Weber 2003; Lecomte et al., 2020). Towards the top of FB1 Fe-carbonates are replaced by Mn-carbonates, these Mn rich black shales are the proto-ore of manganese ore deposits in the area (Dutkiewicz et al., 2007; Gauthier-Lafaye & Weber 1989; Lecomte et al., 2020). The FB2 member is also known as "Poubara sandstone" that is interpreted as turbitide deposits formed during a drop of the water column preceding the formation of FC (Weber et al., 2016). The FC formation comprises dolomites and stromatolitic cherts deposited in a shallow environment and marks an interval between marine incursions (Dutkiewicz et al., 2007; Gauthier-Lafaye & Weber 2003). FD formation is composed of organic-rich black shales with tuffs (Bankole et al., 2015; Gauthier-Lafaye & Weber 2003; Weber et al., 2016). The FE formation is mainly present in the northern part of the Okondja basin and it consists of coarse, cross-bedded, arkose sandstones and interlayered shales (Gauthier-Lafaye & Weber 1989; Weber et al., 2016).

The Francevillian has only undergone minor metamorphism. Modest deformation can be observed as open folds cut by high-angle faults. Estimated post-depositional temperatures of 150 – 250 °C, occasionally 300 °C, evident of a sub-greenschist grade metamorphism of sediments (Lecomte et al., 2020; Lekele Baghekema et al., 2017; Mossman et al., 2001; Ossa Ossa et al., 2013; Yoshida et al., 2024).

Zircon dating of the N'goutou Complex granite intrusion constrains the depositional age of the FA and FB at 2191 ± 13 Ma (Sawaki et al., 2017). U-Pb datings of FD formation detrital zircons and a tuff bed constrain its age between 2072 ± 29 Ma (Thiéblemont et al., 2009) and 2003 ± 16 Ma (Weber et al., 2016), respectively.

3. Raman Spectroscopy

3.1 The Raman Effect

When light hits a molecule, a number of interactions may take place. In the case of infrared absorption, the molecule absorbs the photon and begins to vibrate; the molecule heats up. A molecule will only absorb photons with certain amounts of energy which matches the energy needed to give a bond a specific vibration. With the Rayleigh scattering interaction, the molecule absorbs and then emits a photon of the same energy, in simple terms it reflects light. Sometimes when a molecule absorbs a photon, it enters a higher energy state and upon returning emits a higher wavelength photon - a process called the Stokes Raman scattering has taken place. This effect was first time observed by C.V. Raman in 1928 and was named after him (Smith & Dent 2004).

Similarly to infrared absorption, the difference in photons' energies during Raman effect matches a bond's vibration. The probability of Raman scattering is low 10^{-6}–10^{-8} (Smith & Dent 2004). When a bond is already vibrating and absorbs a photon it is possible a photon of higher energy might be emitted, in this case the anti-Stokes Raman scattering is observed which is identical to the Stokes Raman scattering but the Raman shifts have negative values.

There exists also a process where after photon absorption non-radiative transitions take place followed by emitting a lower energy photon, this process is called fluorescence. Certain compounds emit fluorescence which may be many times stronger than the Raman effect.

Typically lasers of a fixed wavelength are used to excite samples to emit a Raman signal. When measuring Raman spectrum the laser is selected so that background fluorescence would be minimal. Typically Raman spectra taken with longer wavelength lasers experience less fluorescence. Also, the longer the laser's wavelength, the more it penetrates the sample to a depth of half the laser beam wavelength (Smith & Dent 2004).

In order to collect Raman spectra a filter is used to cut out the original laser wavelength so that only photons with a longer wavelength reach the CCD detector (Figure 3). Two types of filters are used. A notch-type filter is used to cut out the laser line, making it possible to observe both the Stokes Raman and anti-Stokes Raman scattering. An edge filter is used to cut out the laser line and the higher wavelengths.

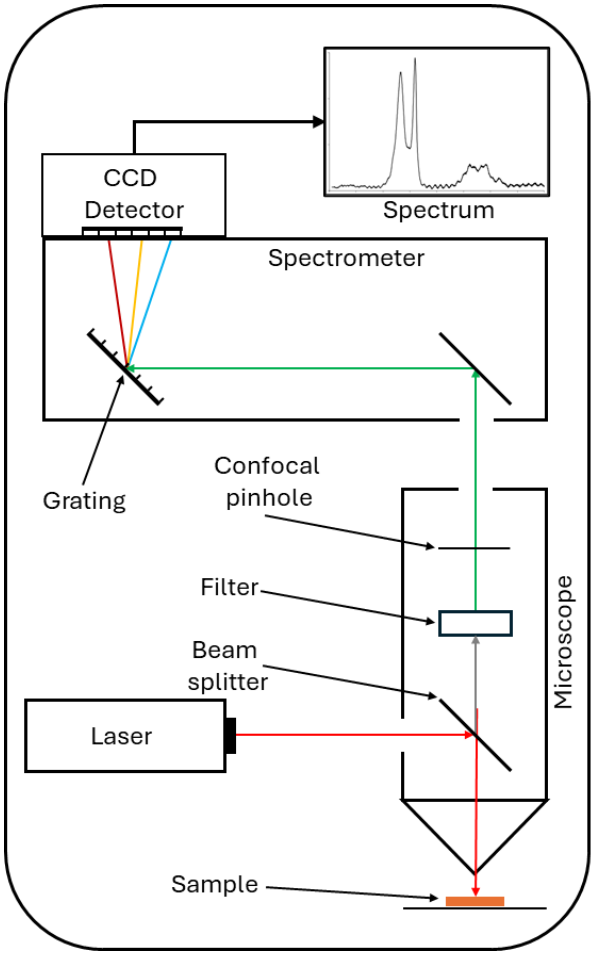

Figure 3. Principal scheme of the Raman spectroscopy system. From Schmid & Dariz (2019).

3.2 Raman Effect in Carbon Materials

Carbon has two main vibrations observable as G and D bands in Raman spectra (Figure 4). First order G band is situated at approximately 1600 cm^{-1}, and the first order D band appears at around 1350 cm^{-1} (Ferrari & Basko 2013). G peak is formed by carbon atoms vibrating synchronously in-plane the benzene ring (Figure 4). The G peak is very intense in the case of graphite and graphene but is absent in pure diamond. The D peak is formed by scissor type vibration in-plane the benzene ring. This peak is intense in pure diamond but is absent in quality graphite and graphene. Both the G and D peaks are present in amorphous and lower crystallinity carbons. Lower crystallinity carbons may have more than one D peak which describe the vibrations of more defective carbon structures. Different schools denote these peaks differently, for example D', D'' etc (Ferrari &

Basko 2013) and D1-D5 (Henry et al., 2019), the latter scheme is used in this study. Side-by-side D vibrations combine and give a higher order Raman shift, such as the 2D peak position (2700 cm^{-1}) is obtained by multiplying the D peak position (1350 cm^{-1}) by two. Very high crystallinity carbon such as graphite and graphene have high intensity 2D peaks. Using the position of 2D peak it is possible to tell the number of graphene layers in the carbon (Ferrari & Basko 2013), and in the 2D peak for graphite there is a significant shoulder peak that stands for graphene.

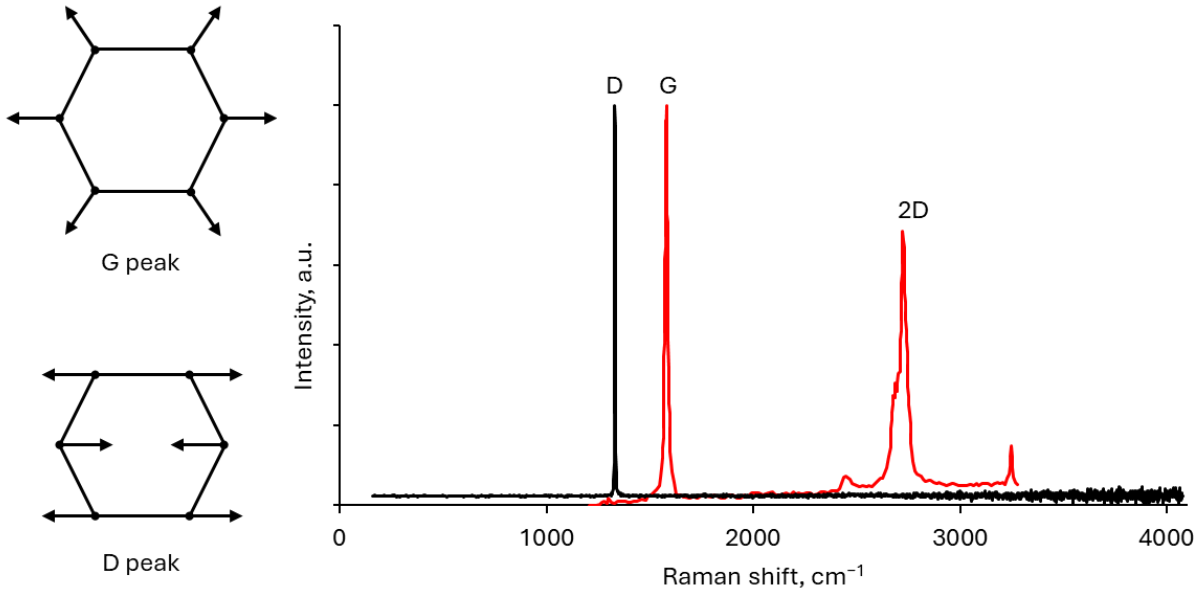

Figure 4. Schematic representation of the vibration in diamond (black) and graphite (red) structures, and the respective G and D bands in Raman spectra. Modified after Ferrari & Basko (2013).

Spectral features such as intensity ratio, area ratio and width (FWHM - full width at half maximum) can be extracted from Raman spectra (Kouketsu et al., 2014). Typically 3 types of functions are used to fit spectra: Lorentzian, Gaussian and Voigt. Generally Gaussian function is good for solids, Lorentzian for gases and Voigt for liquids. However, in the case of graphenes Lorentzian is most commonly used (Ferrari & Basko 2013) but in the case of carbonaceous material Lorentzian or pseudo-Voigt functions are used (Ferralis et al., 2016; Kaneki & Kouketsu 2022; Kouketsu et al., 2014).

4. Materials and methods

4.1 Sample preparation

Samples were selected to obtain as wide a stratigraphic and lateral distribution of the organic rich samples in the basin as possible. Both drillcore and outcrop samples were selected from different stratigraphic levels. Prior TOC analyses were relied upon when applicable to select organic rich samples. In geological sections with no such prior data selection was done visually based on coloration and rock type while providing the best stratigraphic distribution possible. Barren gray shales and pale sandstones were omitted from selection. Where possible existing thin sections were used, else polished sections were prepared for analysis or pieces of pyrobitumen were analysed directly. In total 35 samples were prepared (Table 1), one from the boundary of FA/FB, 16 from FB, six from FB/FC and 12 from FD formations (Figure 1, 2). Out of these four were outcrop samples, one from FD and three from FB formation. The FA sample along with all FB samples originate from Franceville basin. 11 samples are from Lastoursville basin out of which six belong to FB/FC formations and five in FD. One FD sample is an outcrop sample from Franceville basin and the remaining six FD samples are from Okondja basin (Figure 1).

In order to make polished sections, first pieces sized suitably for analysis were cut from the rocks using a table diamond saw. Cuts were made close to or perpendicular to the bedding. These pieces were then dried and placed in moulds before pouring epoxy and left to harden. After hardening a plane suitable for analysis was wet polished using a rotating table polishing machine. Grinding was carried out until grit rating P2000. Some thin sections were coated with carbon for scanning electron microscope analysis, so this coating was carefully removed with 1 μm polishing solution by hand. Additionally, they were cleaned in an ultrasonic bath for 30 seconds to remove any carbon coating residues.

Table 1. Background information for analysed samples.

Sample name	Stratigraphy	Lithology	Sub-basin	Drillcore/ outcrop
9700-14	FA/FB	conglomeratic sandstone	FRV	Sully
AMD4	FD	gray shale	OK	AMD
AMD13	FD	gray shale	OK	AMD
AMD20	FD	black shale	OK	AMD
AMD27	FD	black shale	OK	AMD
AMD32	FD	black shale	OK	AMD
AMD96,62	FD	black shale	OK	AMD
BGB60	FB	pyrobitumen vein / shungite	FRV	BGB60
BNFD1	FD	black shale	FRV	BN
DM11	FD	gray shale	LST	DM
DM34	FD	black shale - dolomarl	LST	DM
DM50	FD	black shale - dolomarl	LST	DM
DM174	FD	gray shale	LST	DM
DM191	FD	black shale - dolomarl	LST	DM
FB35,5	FB	black shale	FRV	FR
FB36,5	FB	black shale	FRV	FR
FB46,2	FB	black shale	FRV	FR
LST12-31,3	FB/FC	black shale	LST	LST12
LST12-35,45	FB/FC	black shale	LST	LST12
LST12-54,25	FB/FC	black shale	LST	LST12
LST12-55,66	FB/FC	black shale	LST	LST12
LST12-61,18	FB/FC	black shale	LST	LST12
LST12-78,7	FB/FC	pyrobitum., brecciated dolostone	LST	LST12
ML594-4	FB	black shale	FRV	ML594
ML594-14	FB	black shale	FRV	ML594
ML594-17	FB	black shale	FRV	ML594
ML605-3	FB	black shale	FRV	ML605
ML605-10	FB	black shale	FRV	ML605
ML605-16	FB	black shale	FRV	ML605
ML605-21	FB	black shale	FRV	ML605
ML605-26	FB	black shale	FRV	ML605
ML605-37	FB	black shale	FRV	ML605
MLD-24-02	FB	black shale	FRV	MLD
MLD-24-41	FB	black shale	FRV	MLD
MLD-24-58	FB	black shale	FRV	MLD

4.2 Petrography

Prepared samples were first studied with scanning electron microscopy (SEM) to confirm the presence of and locate organic material (OM) within the sample. The SEM used for imaging was a ZEISS EVO MA15 SEM. Imaging was conducted under variable pressure. Presence of organics was confirmed employing an Oxford AZTEC-MAX energy-dispersive spectroscopy (EDS) detector. OM in the samples was differentiated from epoxy using the same EDS by checking for the presence of Cl found in epoxy but absent in ancient organic matter. On each sample one site was chosen so that it would be large enough to host a laser beam (~1 μm) and also be found using an optical microscope used to aim the laser. Coordinated image maps of sites were made so later navigation would be possible.

4.3 Organic Carbon C-isotope Composition

Stable C isotope ratios (δ^{13}Corg) in organic matter were measured using a Thermo Scientific Delta V Advantage and Thermo Scientific Delta V Plus continuous flow isotope ratio mass-spectrometers (IR-MS) in decarbonated samples. The δ^{13}Corg values of organic matter in samples from LST12 drillcore were previously reported in Mayika et al. (2020). All carbon isotope results are reported in standard delta notation as *permil* deviation from the Vienna-Pee Dee Belemnite (VPDB) standard: $\delta^{13}C = ({}^{13}R_{sample}/{}^{13}R_{VPDB} - 1)$. Accuracy and precision were monitored via replicate analysis of laboratory and international standards (IAEA-CH-3 $\delta^{13}C$ = -24.72 ± 0.04‰ VPDB and IAEA-CH-6 $\delta^{13}C$ = -10.45 ± 0.03‰ VPDB). Reproducibility was better than ± 0.2‰ for $\delta^{13}C_{org}$.

4.4 Raman Measurements and Spectral Analysis

Raman spectra were taken using Renishaw inVia Raman Microscope at the Institute of Chemistry, Tartu University, equipped with a Peltier-cooled CCD detector and 1200 lines/mm grating. In this study 633 nm wave-lenght He-Ne laser line was used. The focusing was performed using a confocal hole through a 50x short distance objective under reflective illumination. The laser spot size was ~1000 nm. Laser power was set at 0.6 mW (5%) in order to avoid burning the sample as the 10% laser power showed visible burning marks. A calibrated edge high band filter was used to minimize the elastic backscatter signal. Spectra were taken between 50 to 4000 cm^{-1} using the synchroscan method where the grating is rotating during spectral collection. The typical

acquisition time was 176 seconds. The software used for taking measurements was WiRE 3.4. A minimum of 2 coinciding measurements were taken per sample, with the average being 5 measurements. Out of multiple acquisitions, measurements with least fluorescence were selected for the calculation of the average spectrum. The background subtraction for the spectra was performed using the cubic spline interpolation technique. Peak fitting was carried out using Fityk software and a Python script for automatic peak deconvolution (Kaneki & Kouketsu 2022). In this study, a pseudo-Voigt peak function was used, which is a linear combination of the Lorentzian and Gaussian functions, as is commonly used in similar applications (Ferralis et al., 2016; Kouketsu et al., 2014). Pseudo-Voigt function allows for quantification of the Gaussian and Lorentzian components's ratios and has proven to be more consistent across different software packages (Turner et al., 2022).

Kouketsu et al. (2014) have proposed a workflow for optimal fitting of Raman spectra for geothermometry of carbonaceous material of various metamorphic grades using mostly pseudo-Voigt functions. Further development of the method was presented in Kaneki & Koutetsu (2022) with more detailed initial conditions for functions before fitting (see Figure 5).

The workflow is based on evaluating characteristics of the spectrum's first-order bands , which are used to select a suitable fitting method. First, by looking at the presence or absence of the D4 peak, the metamorphic temperature range can be estimated either as lower or higher than ~340 °C. In the case of absence of the D4 peak the spectrum may be fit without fixing parameters and fitting is performed with the the D1, D2, D3 and G peaks as present in the spectrum. However, in the case of lower metamorphic grade organic matter, two additional operations must be conducted to reach the best fitting method.

First, the possibility of having a unique fit using five bands must be considered. If a unique solution is possible, the spectrum may be fitted using bands D1, D2, G, D3 and D4 with the latter fixed at 1245 cm^{-1}. Initial position for the D1 peak is set in the spectral range of 1320 – 1400 cm^{-1} and initial peak intensity is set at 90% of the maximum with FWHM set to 65 cm^{-1}. G band is set similarly between the spectral range of 1580 – 1600 cm^{-1} with FWHM set to 40 cm^{-1}. For D2 and D3 bands the residual spectrum is considered with peak intensity set at the maximum residual spectrum within the 1610 – 1630 cm−1 and 1500 – 1540 cm−1 spectral ranges, respectively. Initial FWHM values for D2 and D3 are set at 30 and 130 cm^{-1} respectively. The D4 band center is fixed

at 1245 cm^{-1} and its initial intensity set equal to the intensity of the residual spectrum at wavenumber closest to 1245 cm^{-1}.

If a unique solution is not found, the intensity ratio of the D2 and D1 peaks must be considered. Ratio of D2/D1 < 1.5 grants the fitting of the G band as a Lorentzian function fixed at 1593 cm^{-1} at the maximum of the residual spectrum with an initial FWHM of 50 cm^{-1}. For peaks D1 and D2, the 90% method is used at ranges within 1320 – 1400 cm^{-1} and 1610 – 1630 cm^{-1} with widths of 80 and 30 cm^{-1}, respectively. D3 and D4 peaks are set as in the previous fitting, with FWHM set at 170 cm^{-1} for both bands instead. When the ratio is larger than 1.5, the G band is omitted from fitting, and a four-peak fit with D1, D2, D3 and D4 bands is used, with D3 fixed at 1510 cm^{-1}. D1 and D2 peaks are fitted again at 90% of the maximum, with D2 this time in the range 1580 – 1650 cm^{-1}. FWHMs for peaks D1 and D2 are to be set at 130 and 55 cm^{-1}, respectively. The D3 and D4 peaks are fixed at 1510 and 1245 cm^{-1} with widths of 170 and 150 cm^{-1}, respectively, with intensities set to the value at the closest wavenumber to the fixed position. The initial shape of all pseudo-Voigt functions is set to 0.5 in all fitting procedures.

In the temperature range of around 150 - 400 °C there is an almost linear correlation between the FWHM values of D1 or D2 bands and paleotemperature. Thus, the paleotemperature can be calculated according to formulas (1) or (2).

T_{D1} (°C) = $-2.30(FWHM_{D1}) + 486$ (1),

where the $FWHM_{D1}$ is the full width at half maximum of the D1 (the main D) band.

T_{D2} (°C) = $-7.01(FWHM_{D2}) + 545$ (2),

where the $FWHM_{D2}$ is the full width at half maximum of the D2 (G) band.

The error for Equation 1 is around ±30 °C and ±35 °C for Equation 2.

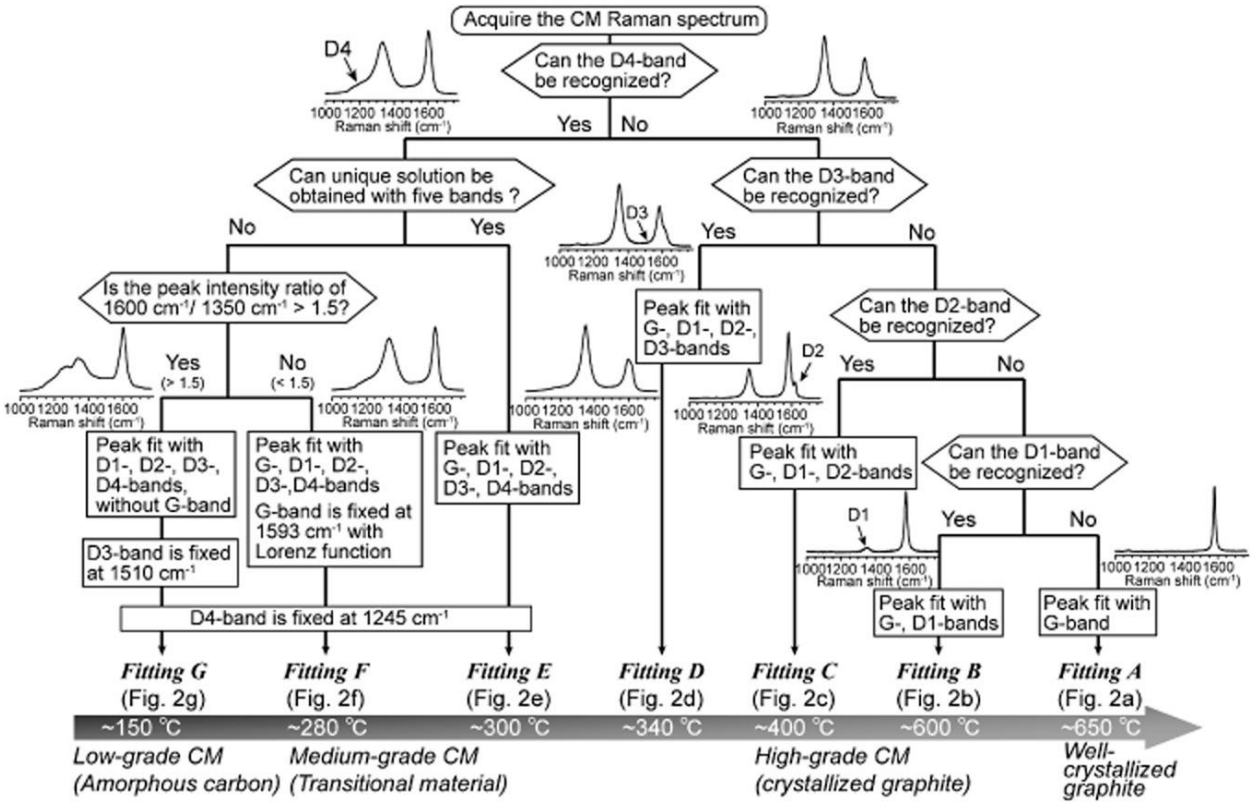

Figure 5. Workflow for choosing the optimal fitting method for geothermometry of carbonaceous material. From Kouketsu et al. 2014.

According to Kaneki & Kouketsu (2022), when fitting spectra, the D2 band is more prone to being altered by the subjective choice of fitting. Thus, it is recommended to fit spectra using Fitting E (Figure 5) and calculate temperatures after D1 band as it is more resilient to being fit incorrectly, and any impact on temperature estimation is less than the uncertainty of the geothermometer itself.

To evaluate H/C (hydrogen:carbon) ratios in studied carbonaceous materials a method described by Ferralis (2016) is used. First, the spectrum is modeled with an up to seven peak fit using pseudo-Voigt profiles. The peaks are denoted as D4, D5, D1, D3, D3′ and G+D2 with initial positions at 1150, 1260, 1330, 1400, 1500, 1580 and 1600 cm^{-1}, respectively. If D2 and G are distinguishable then two separate peaks are modeled. Peaks at 1400 and 1500 may be modeled as a single peak. Peak width is limited to 100 cm^{-1}.

There is a strong linear correlation (3) between the areas of the D5 and G+D2 bands and H/C ratios.

$$H/C = 0.871 \cdot I_{D5} / I_{G+D2} - 0.0508 \quad (3),$$

where I_{D5} is the integrated intensity (area) of the D5 peak and I_{G+D2} is the area of the combined G and D2 peaks.

If D4 and D5 bands are fitted with one peak, a different correlation (4) is used:

$H/C = 0.6024 \cdot (I_{D4} + I_{D5})/I_{G+D2} - 0.0739$ (4),

where I_{D4} is the area of the D4 peak.

In high maturity materials where H/C is less than 0.15 Equation 4 is found to be more reliable (Ferralis 2016).

5. Results

5.1 Petrography

The host rocks of the studied OM ranged from conglomeratic sandstone to gray shales and carbonates (Table 1). FA/FB sample is from a contact between a medium, poorly sorted sandstone and a gravelly conglomerate. Quartz in the conglomeratic sandstone is rounded to subrounded and the rock contains 1 – 5 mm rounded pyrobitumen clasts and some angular mudstone clasts (Figure 6). Samples from FB formation were mostly taken from organic rich black shales. One sample from FB was from a pyrobitumen/shungite vein from Bagombe (BGB) drillcore. Samples from FB/FC were taken from black shales and brecciated dolostones interpreted as paleokarst features (Mayika et al., 2020) with quartz and calcite sealing the pyrobitumen fragments containing veins. FD formation samples from Okondja and Lastoursville sub-basins are represented by black shales and paler gray shales. Some FD black shale samples, specifically from Doume (DM), also contained dolomarl interlayers.

Figure 6. Different host rock for samples. Black shales of MLD and ML594 drillcores, brecciated dolostone from LST12 and conglomeratic sandstone in Sully drillcore, sample S-9700.

Several forms of OM were observed across samples (Figure 7) – (a) migrated pyrobitumen filling secondary porosity, (b) migrated pyrobitumen in brecciated limestones, (c) migrated pyrobitumen filling earlier hydrothermal veins, and (d) potentially *in-situ* organic material in black shale.

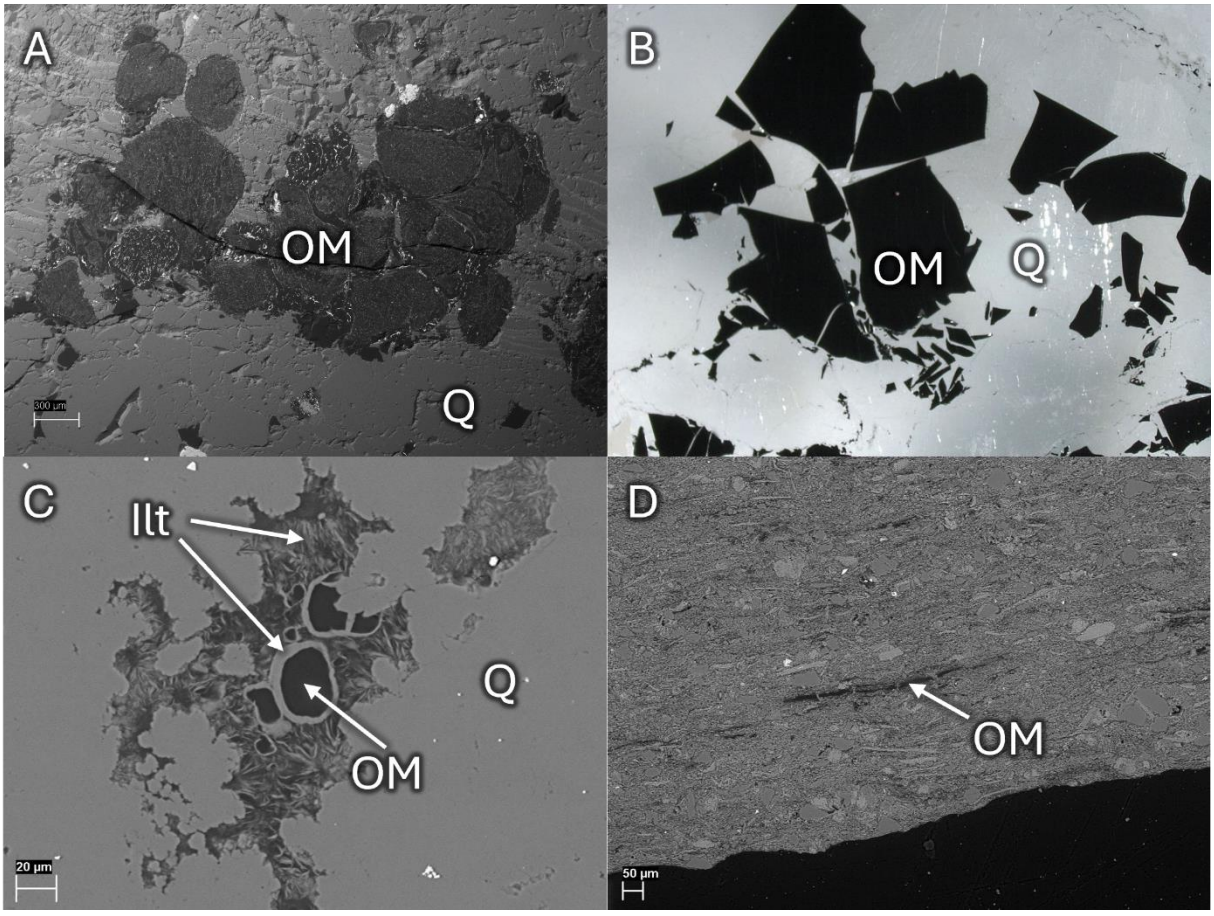

Figure 7. Different forms of organic material (OM) observed across the samples. Ilt – illite, Q – quartz. (a) Nodules of uraniferous bitumen in sample 9700-14; (b) Brecciated OM in quartz matrix of LST12-78,7; (c) Globules of OM with illite rim inside quartz in LST12-31,13; (d) OM lamellae in MLD-24-58.

In the sample from the FA sandstones in the Francevillian sub-basin, the organic material was present in the form of round uraniferous pyrobitumen nodules/fragments filling the secondary porosity of the coarse conglomeratic sandstone host rock and representing ancient migrated oil. Similarly, the migrated pyrobitumen was present in the sample of brecciated FB/FC carbonate in LST12 drillcore from Lastoursville sub-basin (Figure 7b). The pyrobitumen in brecciated limestones occurs as angular, shard-like pieces of OM in the silica and late calcite-filled veins. Petrographic relationships indicate that the pyrobitumen-filled fractures in this succession were

formed before the late calcite and quartz mineralisation that was emplaced into the solidified pyrobitumen.

In addition, organic matter can be observed as globules within silicified rocks, whereas typically these globules also show illite/mica rims (Figure 7c). Similarly, in some quartz veins rich in euhedral pyrite crystals, the OM fills gaps between pyrite aggregates or, on some occasions, OM fills the space left by dissolved minerals. In both cases, the petrographic relationships indicate that the OM in these rocks occurs as pyrobitumen, migrated later than or synchronously with the veining, involving some hydrothermal activity before or during the migration of hydrocarbons.

Potentially in-situ organic material is present in FB and FD formation black shales, where OM occurs as lamellae parallel to the overall layering of the host rock. Lamellae are elongated along the bedding with lengths varying between a few tens of microns to some reaching 500 μm and longer. The thickness of lamellae is less variable and typically does not exceed 10 μm (Figure 7d)

5.2 $\delta^{13}C_{org}$ composition

The $\delta^{13}C$ values of bulk organic material in the studied samples varied between -23.55 to -48.3‰ (Table 2). The pyrobitumen in FA/FB sandstone shows a value of -26.13‰ (Figure 8). In FB black shale the $\delta^{13}C_{org}$ values were from -30 to -34.4 ‰, but two samples from Mouléndé (MLD) core differed considerably showing values at -25.82 and -23.55‰. The $\delta^{13}C_{org}$ values of FB/FC samples from Lastoursville sub-basin varied between -35.06 and -46.27‰. The FD samples' $\delta^{13}C_{org}$ values varied the most, ranging from -35.6 to -48.3 ‰.

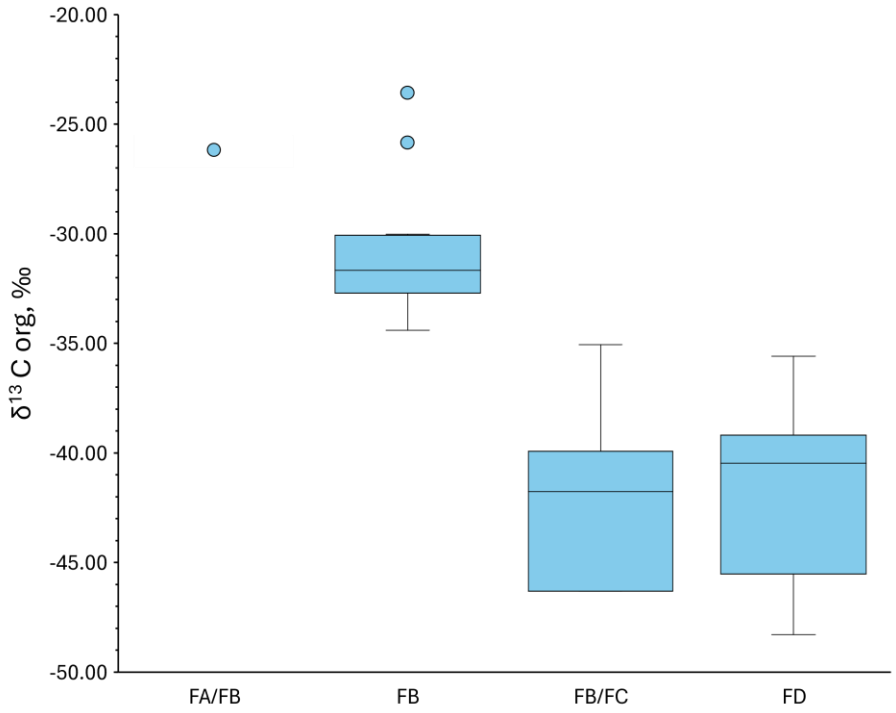

Figure 8. Variation of the $\delta^{13}C_{org}$ values in different stratigraphical units.

Table 2. Calculated temperature (T), hydrogen to carbon (H:C) ratio, measured $\delta^{13}C_{org}$ values and observed organic material (OM) type. The $\delta^{13}C_{org}$ values of outcrop samples were not measured, and sample ML605-10 contained carbonate and was discarded.

Sample	**Formation**	**T, °C**	**H:C**	**$\delta^{13}C_{org}$, ‰**	**OM type**
9700-14_1	FA/FB	204	0.18	-26.13	Pyrobitumen
AMD4	FD	285	0.41	-35.59	In-situ
AMD13	FD	279	0.22	-40.31	In-situ
AMD20	FD	270	0.22	-37.49	Pyrobitumen
AMD27	FD	297	0.38	-40.70	In-situ
AMD32	FD	263	0.50	-40.44	In-situ
AMD96,62	FD	272	0.02	-39.18	In-situ
BGB60	FB	290	0.22	-34.40	Pyrobitumen
BNFD1	FD	272	0.47	-	In-situ
DM11	FD	275	0.59	-45.53	In-situ
DM34	FD	236	1.15	-40.47	In-situ
DM50	FD	250	1.09	-41.70	In-situ
DM174	FD	260	1.11	-46.58	In-situ

DM191	FD	268	0.37	-48.29	In-situ
FB35,5	FB	299	0.42	-	In-situ
FB36,5	FB	266	0.14	-	In-situ
FB46,2	FB	272	0.26	-	In-situ
LST12-31,3_1	FB/FC	256	0.28	-46.30	Pyrobitumen
LST12-31,3_2	FB/FC	259	0.42	-46.30	Pyrobitumen
LST12-35,45	FB/FC	269	0.28	-46.27	Pyrobitumen
LST12-54,25	FB/FC	260	0.42	-41.76	Pyrobitumen
LST12-55,66	FB/FC	255	0.29	-41.29	In-situ
LST12-61,18	FB/FC	284	1.15	-39.93	Pyrobitumen
LST12-78,7	FB/FC	263	0.39	-35.06	Pyrobitumen
ML594-4	FB	281	0.60	-32.19	In-situ
ML594-14	FB	287	0.35	-30.21	Pyrobitumen
ML594-17	FB	288	0.15	-32.16	In-situ
ML605-3	FB	287	0.48	-30.17	In-situ
ML605-10	FB	288	0.04	-	In-situ
ML605-16	FB	289	0.44	-31.17	In-situ
ML605-21	FB	291	0.38	-30.02	Pyrobitumen
ML605-26	FB	285	0.79	-32.74	In-situ
ML605-37	FB	293	0.72	-32.75	In-situ
MLD-24-02	FB	296	0.66	-32.57	In-situ
MLD-24-41	FB	210	0.31	-25.82	In-situ
MLD-24-58	FB	277	0.36	-23.55	In-situ

5.3 Raman spectroscopy

A total of 36 Raman spectra were acquired from 35 samples. Notably, spectra from the same formation are similar in shape, while spectra of different formations differ mostly by the shape of the D4 peak (Figure 9). Exceptions are samples from FD formation where Ambinda (AMD) core samples differ slightly from FD formation samples from Doume (DM) core.

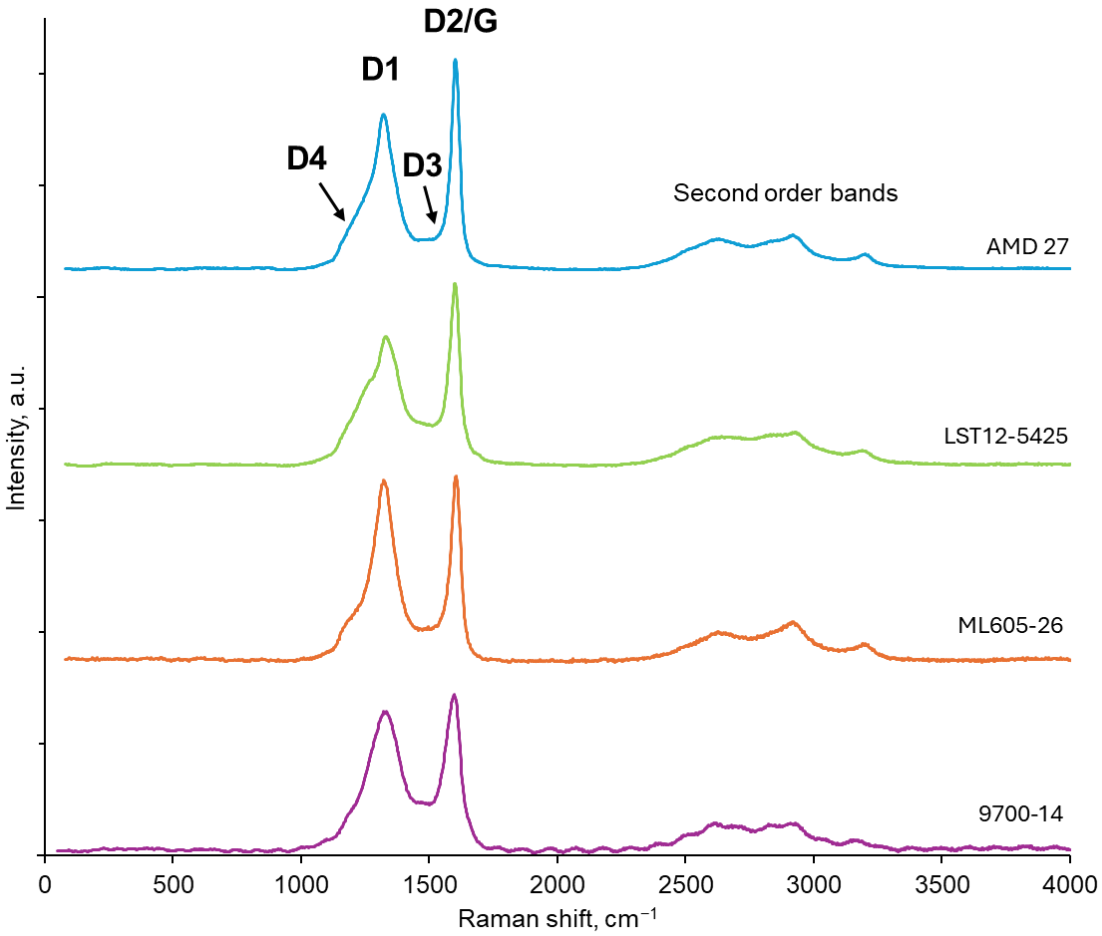

Figure 9. Comparison of normalized Raman spectra. 9700-14 from FA/FB, ML605-26 from FB, LST12-5425 from FB/FC and AMD27 from FD formation.

In all studied samples, a unique solution with the best fit between the measured and modelled spectrum was achieved using five bands - D1, D2, G, D3 and D4 (Figure 10). In order to avoid subjectivity in results, all spectra were fitted using the method recommended by Kaneki & Koutetsu (2020) (Figure 10b). Initial position for D1 peak was set at the peak in the spectral range of 1320 – 1400 $cm^{-1,}$ and initial peak intensity was set at 90% of the maximum with FWHM set to 65 cm^{-1}. G band was set similarly between the spectral range of 1580 – 1600 cm^{-1} with FWHM set to 40 cm^{-1}. For D2 and D3 bands the residual spectrum was considered with peak intensity set at the maximum residual spectrum in spectral ranges of 1610 – 1630 cm^{-1} and 1500 – 1540 cm^{-1} respectively. Initial FWHM values for D2 and D3 were 30 and 130 cm^{-1}, respectively. The D4 band center was fixed at 1245 cm^{-1} and its initial intensity was set at the intensity of the residual

spectrum at wavenumber closest to 1245 cm^{-1}. With this method, only temperatures calculated after the D1 band and Equation 1 are considered reliable (Kaneki & Koutetsu, 2020).

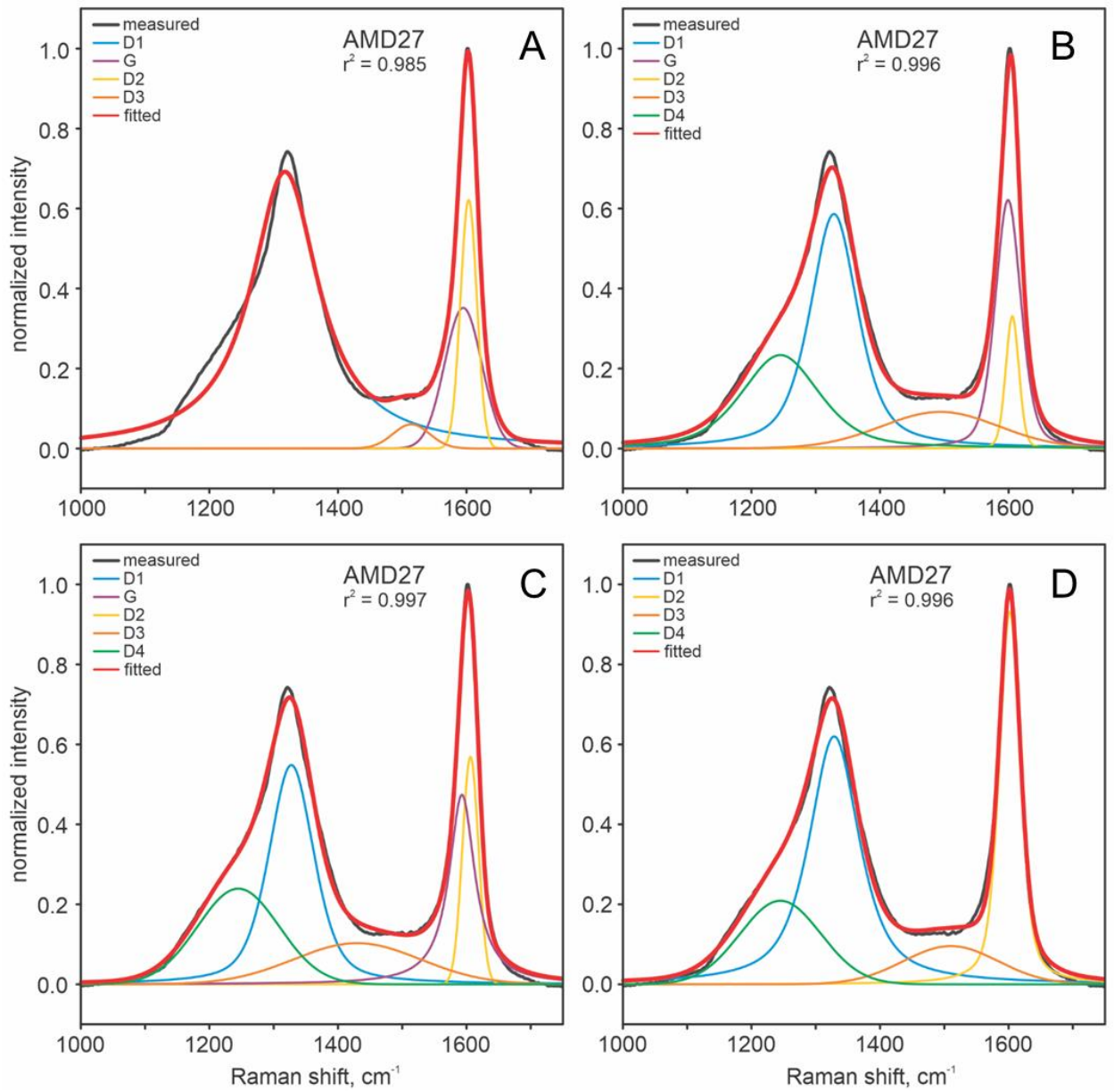

Figure 10. Examples of the sample AMD27 spectra fitting with different bands and fitting strategies. In (a), no bands were fixed; in (b) – (d), the D4 band is fixed at 1245 cm^{-1}; additionally, in (c), the G band is modelled with a Lorentzian distribution function and is fixed at 1593 cm^{-1}; in (d), the D3 band is fixed at 1510 cm^{-1}.

Overall, the positions of the center for the D1 band varied between 1325 and 1340 cm^{-1}. Center positions of D1 peaks appear to group based on basin - positions of D1 from Lastoursville sub-

basin samples differed significantly from the other two basins (Appendix 1) The center for Lastoursville samples varies between 1337 – 1341 cm^{-1}. In Okondja sub-basin samples center position varied between 1328 – 1334 cm^{-1}, and in Franceville sub-basin center position varied between 1325 – 1334 cm^{-1}, with 50% of values between 1327 – 1330 cm^{-1}.

Variability of D2 band center positions was from 1596 to 1617 cm^{-1} (Appendix 1). FA sample had the lowest value of 1596 cm^{-1}. Values for the FB formation remained between 1604 – 1607 cm^{-1}, with one sample with a central position significantly lower than others at 1598 cm^{-1}. Contrary to D1 center positions, where values were quite similar, the FB/FC samples' center position of D2 varied from 1597 to 1617 cm^{-1}.

The FWHM of the D1 band of measured samples varied from 81 cm^{-1} to 122 cm^{-1} (Appendix 1). The widest D1 peak belonged to the sample from FA. For samples from FB formation FWHM varied between 81 cm^{-1} and 95 cm^{-1} with one sample as an outlier with a FWHM of 120 cm^{-1}. FB/FC samples had FWHM values of 88 – 100 cm^{-1}. FD formation measurements varied more than other formations between 82 – 108 cm^{-1}. As with the center positions, the variations of FWHM were tied to basins, with Lastoursville standing out from Franceville and Okondja sub-basins. Lastoursville samples had values between 88 and 108 cm^{-1} with a median of 98 cm^{-1}. The Okondja sub-basin samples had values from 82 to 97 cm^{-1} and a median FWHM of 93 cm^{-1}. In Franceville sub-basin samples, the D1 band FWHM values varied between 81 and 95 cm^{-1} with the median being 86 cm^{-1}. The Franceville sub-basin samples also had two outliers with FWHM values of 120 and 122 cm^{-1}.

Generally, the variability of D2 band FWHM values was less than that of D1, with a range of 34 cm^{-1} for D2 *versus* a range of 41 cm^{-1} for D1, with FWHM ranging from 12 – 46 cm^{-1}. FA formation again had the widest peak of 46 cm^{-1}. FB formation samples' FWHM measured between 31 and 44 cm^{-1}. FB/FC samples varied the most between 12 – 39 cm^{-1}. In FD formation, the measured D2 band FWHM values stayed between 23 and 38 cm^{-1}. Differences between the sub-basins was not as pronounced. Okondja and Lastoursville basins had similar median FWHM values, 31 and 32 cm^{-1}, respectively. Franceville sub-basin stood out somewhat with a median value of 35 cm^{-1}.

5.4 Estimated Paleotemperatures and H:C ratios

Paleotemperatures were calculated based on the fitted D1 band data. Temperatures calculated after the D1 band varied between 204 and 299 °C (Table 2, Figure 11) The lowest estimated temperature, 204 ± 30 °C, belonged to FA/FB migrated pyrobitumen sample. In FB samples, the calculated temperatures mostly varied between 266 and 299 ± 30 °C, only one anomalous FB sample had a temperature of 210 ± 30 °C. The FB/FC samples' temperatures varied from 256 to 284 ± 30 °C, and FD formation had a larger variation with the lowest result of 236 ± 30 °C and the highest of 297 ± 30 °C.

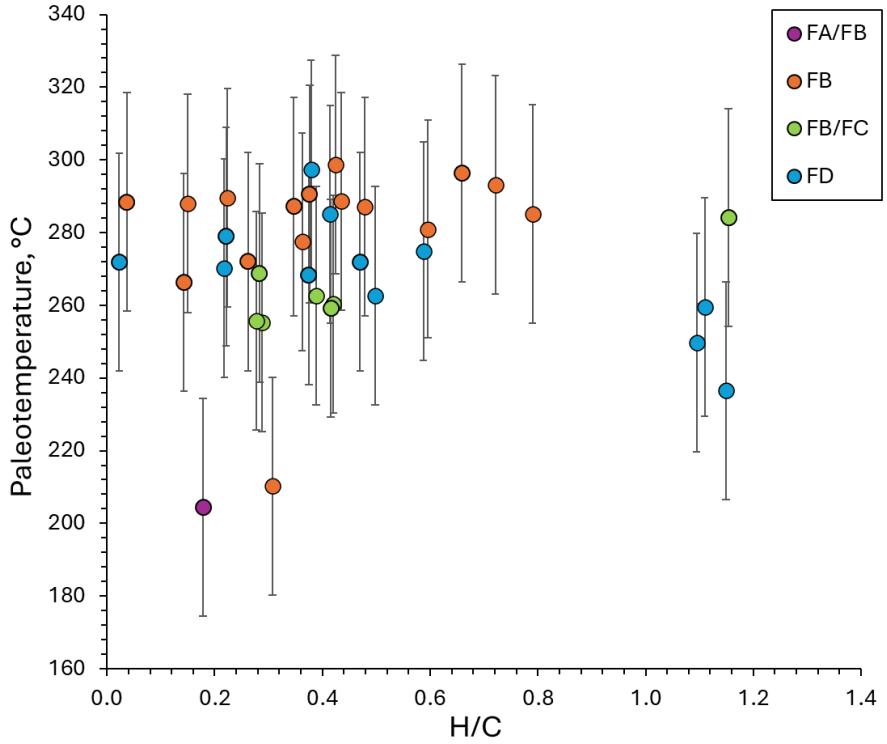

Figure 11. Estimated paleotemperature vs H/C ratio of the organic matter in studied samples.

For H:C ratios, a separate fitting was performed as described above in the Materials and Methods section. In samples analysed, the calculated H:C ratio varied between 0.0226 and 1.1538 when calculated using the area of the modelled D5 band and 0.0182 and 1.3587 when calculated using the sum of integrated intensities of D4 and D5. As there were few samples with H:C ratios less than 0.15, the results of Equation (3) were considered. There was no correlation between measured

paleotemperatures and H:C ratios (Figure 11), nor between paleotemperatures and bulk C-isotope composition, or between H:C ratio and $\delta^{13}C_{org}$ values (Figure 12).

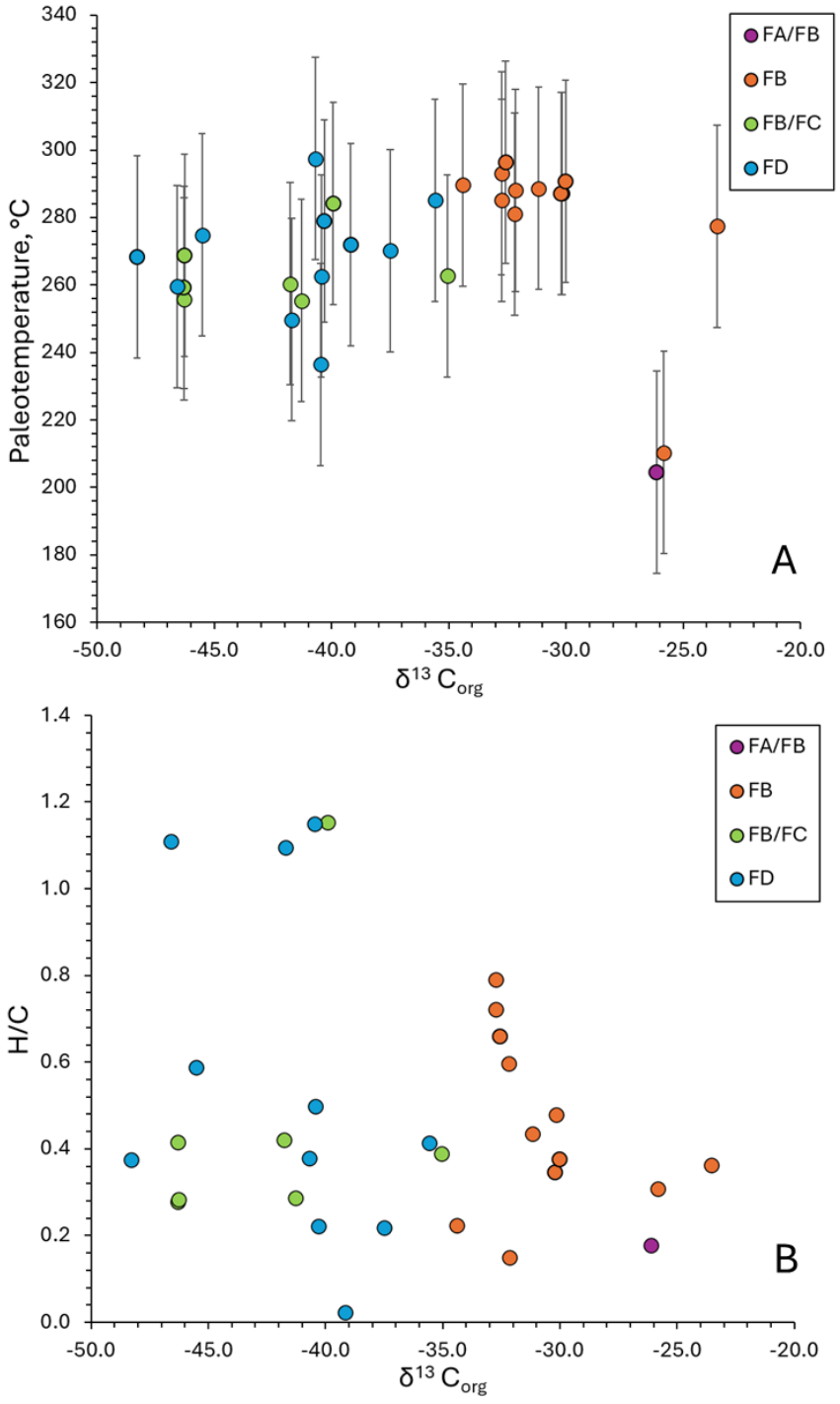

Figure 12. (a) Estimated paleotemperatures vs bulk C-isotope composition of the organic matter; (b) H:C ratios vs bulk organic matter $\delta^{13}C_{org}$ values.

Stratigraphically the paleotemperatures in samples assigned to FB formation vary between 266 and 299 °C with median temperature of 288 °C. It is noteworthy that these results agree with measurements from FB formation microfossils, where temperatures nearing 300 °C were obtained (Lekele Baghekema et al., 2017).

In FD formation samples the paleotemperatures vary 62 °C between 236 – 297 ± 30 °C. An outcrop sample from Franceville sub-basin shows a paleotemperature of 272 °C and FD formation samples in Okondja sub-basin vary between 263 and 297 ± 30 °C (median 275 °C), whereas samples from Lastoursville sub-basin show a temperature range of 236 – 275 ± 30 °C (median 260 °C) (Figure 13). The temperature variance of Franceville basin samples was from 266 to 299 ± 30 °C, quite similar to Okondja.

Generally, the H:C values for samples stayed below 0.8, with the exception of some samples with a H:C ratio above 1. All samples with the high H:C ratio were from the Lastoursville sub-basin (Figure 14), with most from the FD formation; one high H:C ratio sample was from Lastoursville (LST12) drillcore. The FA/FB sample had H:C ratio of 0.18. Samples from FB formation show values from 0.04 – 0.79. The FB/FC samples mostly varied modestly between 0.28 and 0.42 but one sample had a H:C ratio of 1.15. H:C ratios in samples from FD formation varied the most, from 0.02 to 1.15. Notably, lower values of FD were mostly from the Okondja sub-basin, 0.02 to 0.50, and higher ratios were from the Lastoursville sub-basin between 0.37 – 1.15.

Furthermore, paleotemperature comparison of pyrobitumen and in-situ organic material shows no co-variation. Temperatures measured for pyrobitumen are 256 – 291 ± 30 °C and 236 – 299 ± 30 °C for in-situ material (Figure 15). Out of the two outlier samples the FA/FB sample 9700-14 is pyrobitumen and FB MLD-24-41 is potentially *in-situ* OM. H:C ratio comparison of pyrobitumens to *in-situ* organic material also does not differentiate between the two (Figure 15). Although, in-situ material measurements showing higher H:C ratios, pyrobitumen can also have higher (>1) H:C ratio.

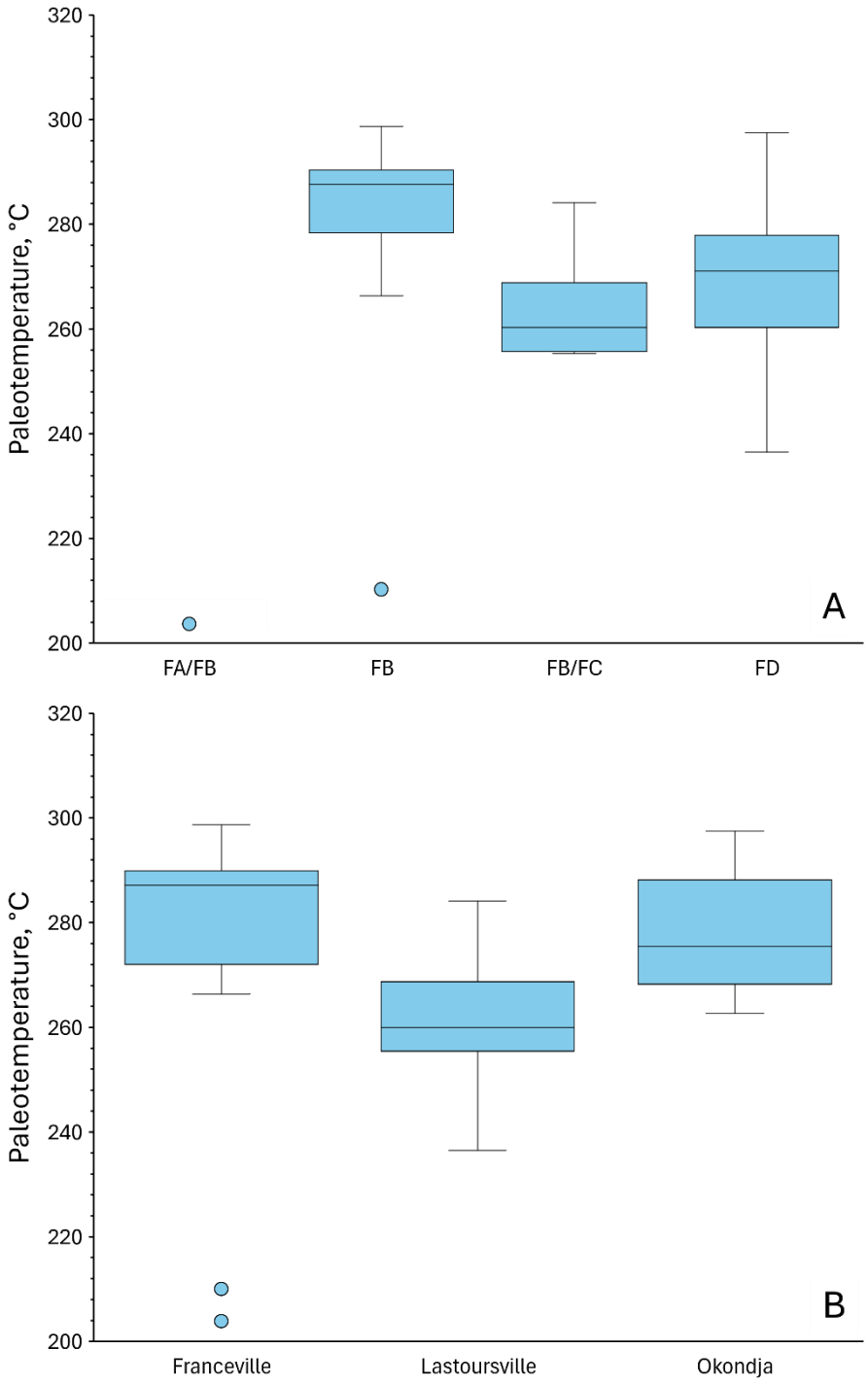

Figure 13. Comparison of Francevillian paleotemperatures' stratigraphic and spatial variation.

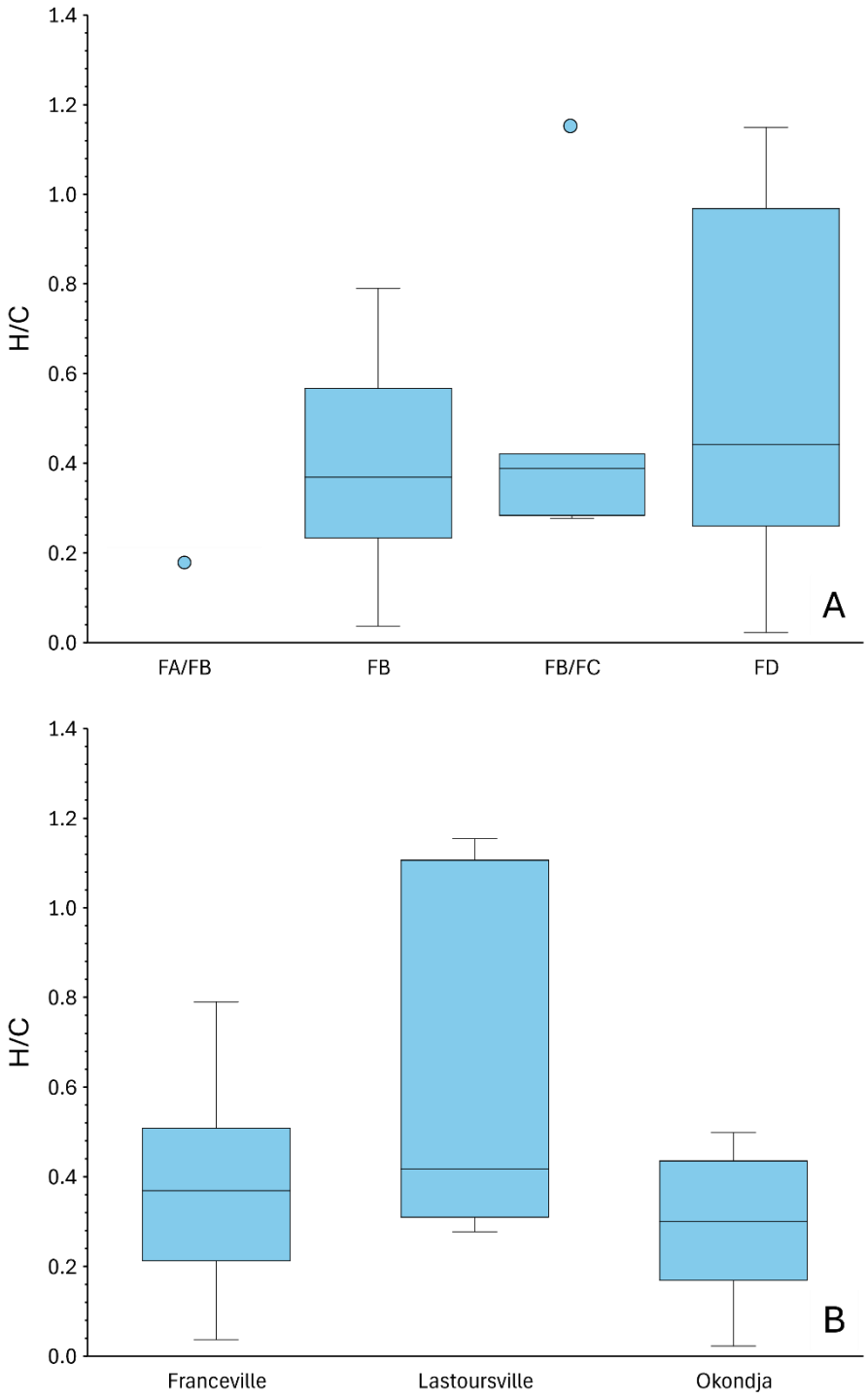

Figure 14. Comparison of Francevillian H:C (hydrogen to carbon) ratios' stratigraphic and spatial variation.

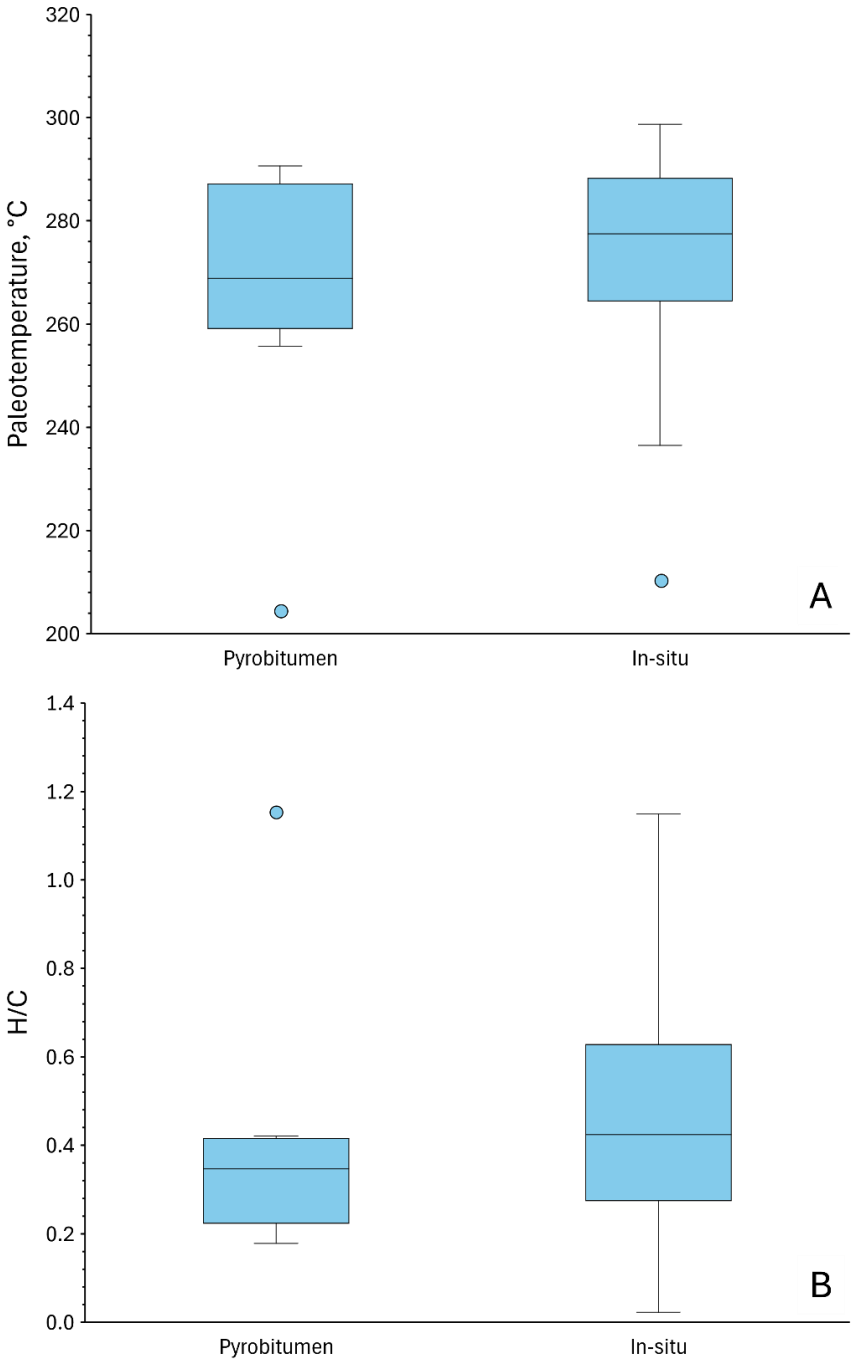

Figure 15. Comparison of pyrobitumen and in-situ organic material variations in temperature and H:C (hydrogen to carbon) ratio.

6. Discussion

Results of this study suggest that paleotemperatures measured from the organic material in the Francevillian Basin were above 230 ± 30 °C but most likely did not exceed 300 ± 30 °C. This thermal alteration was regional, and the paleotemperatures did not vary depending on either stratigraphy or type of carbonaceous material. There is, however, a moderate spatial variation between the Franceville, Lastoursville and Okondja sub-basins' temperatures.

These results generally agree with the previous geothermometry studies of the Francevillian Basin, which, however, have mostly focused on the uraniferous FA formation, especially near the Oklo natural nuclear fission reactors (Dutkiewicz et al., 2007; Gauthier-Lafaye & Weber, 1989; Lecomte et al., 2020; Mathieu et al., 2000; Ossa Ossa et al., 2014).

Two types of bitumens have been observed in FA sandstones (Lecomte et al., 2020). Angular bitumens are located within the rock's primary porosity, trapped in quartz overgrowths or in the residual space between the overgrowths. These angular bitumens are either synchronous with, or later than, the silicification of the formation and are barren of uranium. Bitumen nodules which may host U and other mineralization are located in the secondary porosity formed by dissolution of the host rock. These nodules have formed during the extensional phase of the Francevillian (Mathieu et al., 2000). Fractures allowed the mixing of meteoric recharge and deeper brines. The mix was then transported to the top of FA due to the compaction of sandstones. Hydrocarbon rich fluids overpressured due to a rapid burial of FB pelites, then migrated downwards, causing uraninite mineralization in these later bitumens (Lecomte et al., 2020). Analysis of fluid inclusion homogenization temperatures in vein quartz of FA sediments shows the temperatures 140 – 180 °C (Gauthier-Lafaye & Weber, 1989) and 130 – 200 °C (Dutkiewicz et al., 2007). Dutkiewicz et al. (2007) also reported a second oil migration episode with temperatures in excess of around 250 °C or even as high as 350 °C. This second episode is interpreted as a consequence of the migration of heated fluids along fractures due to the nuclear activity of a reactor ~250 m away from the sampled locality.

However, fluid inclusion data, from ca 30 km from the Oklo reactors, by Mathieu et al. (2000), reports a low saline (2.2 – 8.5 wt% NaCl eq) aqueous solution with homogenization at 190 – 210 °C. Similar results were obtained using clay mineral geothermometry, which also suggests a widespread fluid activity in the FA formation synchronous with oil migration and formation of U-

bearing phases with average temperatures inferred to be ~240 ± 30 °C (Ossa Ossa et al., 2014). Furthermore, chlorite geothermometry by Lecomte et al. (2020) applied to authigenic Fe-chlorites in Mikouloungou and Bangombé uranium deposits close to the FA-FB boundary suggested paleotemperatures between 205 ± 21 °C and 195 ± 41 °C, in-line with results of earlier studies of fluid inclusions. Lecomte et al. (2020) also noted that temperatures for Okélobondo samples show higher values (289 ± 46 °C), which were thought to be caused by nearby natural nuclear reactors, but it has been considered that the thermal oreole of these natural nuclear reactors was limited to 50 (250) m, and the reactors did not have any significant effect on the regional diagenetic-metamorphic grade of the Francevillian (Dutkiewicz et al., 2007; Gauthier-Lafaye & Weber, 1989; Mathieu et al., 2000).

Nevertheless, the results of this study measured from successions hundreds of kilometers away the natural reactors still agree with paleotemperature estimates for FA formation sediments at the reactor surroundings. This might suggest that the first and the latter represent regional paleotemperature levels that do not depend on stratigraphy or type of carbonaceous material. Though no geothermometric studies have been conducted reporting data of FD formation, previous Raman geothermometric analyses of Francevillian FB formation microfossils suggest temperatures of 296 ± 30 °C (Lekele Baghekema et al., 2017) similar to the high estimates of this study. Similarly, the black shales of FB are characterised by low H:C and O:C ratios (Dutkiewicz et al., 2007) whereas the reflectance measurements show maximum reflectance of 5.9 – 6% and 5.88 – 6.92% in sapropelic kerogen and bitumen, respectively (Cortial et al., 1990; Mossman et al., 2001) which suggests a meta-anthracite stage corresponding to a (very) low grade metamorphism.

Gauthier-Lafaye and Weber (1989) estimated that the burial depth reached for FA sediments in Francevillian sub-basin was about 4000 m. Lecomte et al. (2020) suggested that maximum burial was achieved already by ca. 2 Ga and caused first oil generation along with first uranium precipitation phases when U-bearing brine interacted with oil expelled from FB formation black shales and became trapped in the FA sandstone reservoirs. The basin burial history was followed by long-lasting uplift, and the 130 °C isotherm was achieved by 250-150 Ma, and the 60 °C isotherm by <165 Ma (Lecomte et al., 2020). It is important that approximately 800-700 Ma ago numerous doleritic dikes of the dike swarm were emplaced during the regional extension in

Francevillian that potentially caused the formation and migration of a generation of additional bitumen (Nagy et al., 1991), and induced galena crystallisation (Mathieu et al., 2000).

The maximum paleotemperature in FA sediments has been typically considered using fluid inclusion data and clay mineral geothermometry at 200 °C (e.g. Gauthier-Lafaye & Weber 1989; Mathieu et al., 2000; Dutkiewicz et al., 2007; Lecomte et al., 2020), which is about 50 to 80 °C lower than estimated from Raman spectroscopy in this study, suggesting paleotemperatures at 250 to 280 °C.

This difference can be, first, due to the ordering of carbonaceous material controlled by the time factor. Though the temperature has the main control on structural ordering of the carbon (e.g., Ferralis et al., 2016), the ordering of the old organic matter, like in the 2 Ga Francevillian sediments, might also be thermodynamically driven.

The second reason can be rooted in the preparation of the samples, as the cutting and polishing can cause elevated temperatures at the sample surface and induce partial graphitisation of the organic matter, resulting in higher paleotemperature estimates (Henry et al., 2019). Although this artefact cannot be fully excluded, extra care was taken to avoid local heating when preparing the samples analysed in this study. Moreover, one of the samples (BGB60) was measured from a broken surface without any polishing but yielded a similar paleotemperature to other samples, which gives confidence in the obtained results.

Interestingly, the lowest Raman paleotemperature of 204 ± 30 °C in this study from FA/FB pyrobitumen sample is similar to chlorite (195 ± 41 – 205 ± 21 °C) and fluid inclusion (190 – 210 °C) thermometry results for sediments away from natural nuclear reactors (Lecomte et al., 2020; Mathieu et al., 2000). Controversially, this suggests that the stratigraphically oldest FA Formation sediments might be the least thermally altered, while paleotemperatures in stratigraphic units above the FA show temperatures considerably higher than 200 °C, reaching nearly 300 °C (Figure 10). However, it should be considered that naturally irradiated bitumens show increased structural disorganisation (Court et al., 2007) that might affect the FWHM values of the carbon bands in Raman spectra and consequently result in apparently lower temperature estimates. Indeed, this pyrobitumen sample shows U-mineralisation in organic matter, casting doubt on this estimate (Figure 16). Furthermore. a similar explanation seems to be valid with respect to an FB sample MLD-24-41, where estimated paleotemperature (210 ± 30 °C) is similarly lower compared to other

samples. In this sample, the measured organic matter surrounds a grain of a Th-rich phosphate mineral monazite that might have had a similar destructuring effect on carbonaceous matter.

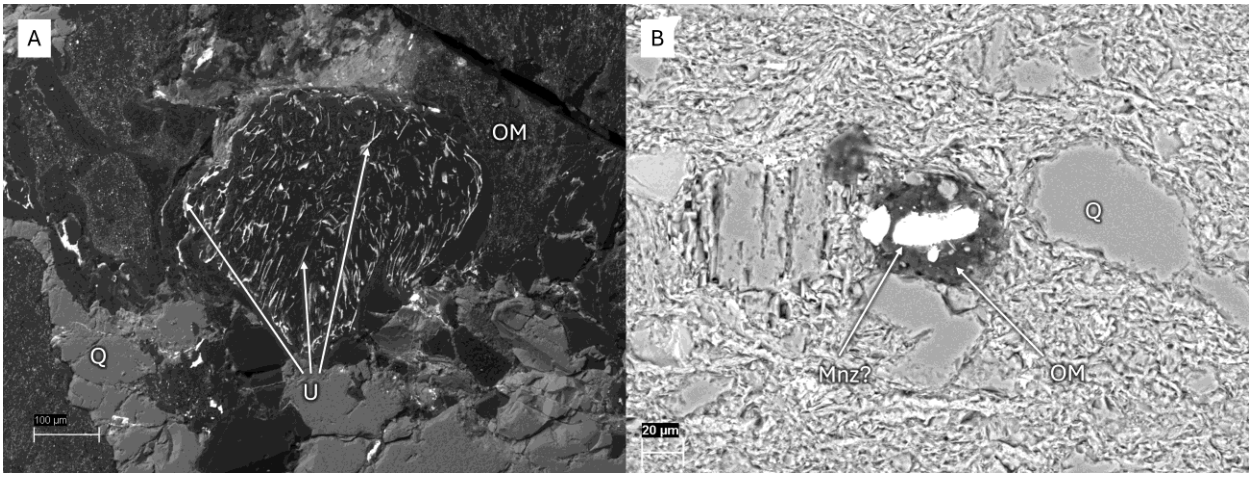

Figure 16. SEM images of organic matter showing anomalously low estimated paleotemperatures. (a) sample 9700-14; (b) MLD-24-41, Mnz - monazite.

Another noteworthy aspect is the apparently lower estimated paleotemperatures in Lastoursville sub-basin compared to Franceville and Okondja sub-basins' paleotemperatures. Also, Lastoursville basin is a less complete and shallower basin than Franceville and Okondja, where the Francevillian is most complete and thickest (Thiéblemont et al., 2009). The maximum burial depth of the Francevillian has been assessed to be 4 000 m at the top of the FA (Gauthier-Lafaye & Weber, 1989). It might be that the burial in Latoursville sub-basin was not as deep and consequently the organic matter shows lower paleotemperatures. Another possible cause for regional thermal alteration is widespread hydrothermal activity. Ossa Ossa et al. (2014) describe such a hydrothermal activity episode coeval with U precipitation in the FA formation which may be connected to nearby volcanic heat sources. The timing of this episode is between 1850 and 2030 Ma (Ossa Ossa et al., 2014). While volcanoclastic rocks have indeed been described in FD and FE formations (Weber, 1968) the only known volcanic sources N'goutou complex is older (2191 ± 13 Ma) and dolerite dykes intruding the Francevillian are considerably younger (1000–800 Ma) (Bonhomme et al., 1982; Sawaki et al., 2017). Moreover, the thermal effect of the up to tens of meters thick dykes remains within tens to maximum hundred meters range.

Ossa et al. (2014) also proposed that the crustal heat flow during the Paleoproterozoic was greater and during the extensional regime and formation of the basin, the lithosphere thinned, causing

higher temperatures in the graben-like Franceville and Okondja basins and lower temperatures in the more horst-like Lastoursville basin.

While the direct cause for the thermal alteration of the Francevillian remains still debatable, it is clear that the organic material in the Franceville, Lastoursville and Okondja sub-basins is above the thermal threshold of 200 °C for the preservation of biomarkers, even though Lastoursville basin has experienced less thermal alteration. One possibility to consider is the lack of information on the Booué sub-basin which is more separate from the rest of the Francevillian, but these sediments are known to be gently folded and subjected to higher metamorphic conditions (Gauthier-Lafaye & Weber 1989).

7. Conclusions

The aim of this master's thesis was to discern the lateral and stratigraphic variability of thermal alteration in organic material and pyrobitumen (solidified petroleum) of the Franceville, Lastoursville and Okondja sub-basins of the Francevillian basin using Raman spectroscopy and reconstruct the extent of thermal overprint on preserved sedimentary organic material by diagenesis-metamorphism, later fluids and magmatism.

Raman spectroscopy is a rapid and non-destructive method to gain insights into the structure and thermal maturity of organic material. In this study analysis of Raman spectra were used for geothermometry of organic material in host rock. Presence of organic material large enough for Raman was confirmed using scanning electron microscopy (SEM).

Temperatures from Franceville, Lastoursville and Okondja sub-basins were calculated from Raman spectroscopy data, covering the Francevillian both spatially and stratigraphically. 35 samples of 10 different drillcores and outcrops from lithostratigraphic units FA, FB, FB/FC and FD were collected and analyzed.

Measured temperatures in the Francevillian exceeded 230°C ± 30°C but remained under 300°C ± 30°C. Spatial variation between the three sub-basins was detected with the lowest temperatures from the Lastoursville basin (236 – 275 ± 30°C). In the Franceville sub-basin, temperatures varied between 266 – 299 ± 30°C, and in Okondja a similar range of 263 – 297 ± 30°C was measured. Stratigraphic variation of temperatures was not detected, implying a regional thermal alteration in the basin.

While the direct cause for the thermal alteration of the Francevillian remains unclear it is evident that the organic material in the Franceville, Lastoursville and Okondja sub-basins is above the thermal threshold of 200 °C for the preservation of biomarkers.

Orgaanilise aines muutumisasme kaardistamine Raman spektroskoopiaga Paleoproterosoilistes Franceville basseini setendites, Gabon

Georg Rahu

Kokkuvõte

Selle töö eesmärk oli Raman spektroskoopia abil uurida Franceville'i basseini Franceville'i, Lastoursville'i ja Okondja alam-basseinide orgaanilise aine ja pürobituumeni (tahkestunud nafta) termilise muutumise lateraalset ja stratigraafilist varieeruvust ning rekonstrueerida säilinud orgaanilise aine muutust diageneesi, moonde, hilisemate fluidide ja magmatismi mõjudel.

Mõnikord kui footon põrkub molekuliga saavutab molekul kõrgema energiataseme ning väljuval footonil on sedavõrd kõrgem lainearv. Seda efekti nimetatekse Stokes Raman efektiks. Raman spektroskoopia abil on võimalik uurida ja kirjeldada süsinikust koosnevate ainete struktuuri ja keemilist koostist, seda võrdlemisi kiirelt ja proovi hävitamata. Süsinikul on kaks põhilist võnkumist mis on spektril vaadeldavad D (1350 cm^{-1}) ja G (1600 cm^{-1}) tippudena. Orgaanilise aine uurimisel on võimalik spektri tunnuste abil hinnata materjali temperatuuri ja vesinik-süsinik (H:C) suhet.

Analüüsiti 35 proovi 10st erinevast puursüdamikust ja paljandist, millega kaeti Franceville'i bassein nii ruumiliselt kui ka stratigraafiliselt. Mõõtmisi tehti lihvitud kivimpaladest ja õhikutest. Skanneeriva elektronmikroskoobiga kaardistati orgaanika levik ning kirjeldati petrograafia.

Selgus, et proovides määratud temperatuurid ei korreleeru H:C suhte, $\delta^{13}C_{org}$ ega stratigraafiaga. Määratud temperatuurid erinesid basseinis ruumiliselt. Franceville'i ja Okondja alambassein olid üsna sarnased (vastavalt 266 – 299 ± 30°C ja 263 – 297 ± 30°C), samas Lastoursville'i alambasseinis olid temperatuurid märgatavalt väiksemad, 236 – 275 ± 30°C,

Üldiselt saab väita, et Franceville'i basseini termilised muutused on lausalised ning regionaalsed, mitte varieeruvad ja lokaalsed. Samuti saab väita, et basseini termilised muutused on olnud biomarkerite säilimiseks liiga kõrged.

Acknowlegdements

I would like to thank my supervisors for their guidance and support throughout the study. I would also like to thank Marian Külaviir for helping with the SEM, Markus Ausmeel, Johanna Maria Ojap, Aivo Lepland and Anthony Prave for their great company during field work, and everyone at Masuku University geology department for the warm welcome.

References

Bankole, O. M., El Albani, A., Meunier, A., & Gauthier-Lafaye, F. (2015). Textural and paleo-fluid flow control on diagenesis in the Paleoproterozoic Franceville Basin, South Eastern, Gabon. *Precambrian Research*, *268*, 115–134. https://doi.org/10.1016/j.precamres.2015.07.008

Bekker, A., & Holland, H. D. (2012). Oxygen overshoot and recovery during the early Paleoproterozoic. *Earth and Planetary Science Letters*, *317*, 295–304.

Bekker, A., Karhu, J. A., Eriksson, K. A., & Kaufman, A. J. (2003). Chemostratigraphy of Paleoproterozoic carbonate successions of the Wyoming Craton: Tectonic forcing of biogeochemical change? *Precambrian Research*, *120*(3), 279–325. https://doi.org/10.1016/S0301-9268(02)00164-X

Bekker, A., Krapež, B., & Karhu, J. A. (2020). Correlation of the stratigraphic cover of the Pilbara and Kaapvaal cratons recording the lead up to Paleoproterozoic Icehouse and the GOE. *Earth-Science Reviews*, *211*, 103389.

Bindeman, I. N., Zakharov, D. O., Palandri, J., Greber, N. D., Dauphas, N., Retallack, G. J., Hofmann, A., Lackey, J. S., & Bekker, A. (2018). Rapid emergence of subaerial landmasses and onset of a modern hydrologic cycle 2.5 billion years ago. *Nature*, *557*(7706), 545–548.

Blank, C. E., & Sanchez-Baracaldo, P. (2010). Timing of morphological and ecological innovations in the cyanobacteria–a key to understanding the rise in atmospheric oxygen. *Geobiology*, *8*(1), 1–23.

Bonhomme, M. G., Gauthier-Lafaye, F., & Weber, F. (1982). An example of lower proterozoic sediments: The Francevillian in Gabon. *Precambrian Research*, *18*(1), 87–102. https://doi.org/10.1016/0301-9268(82)90038-9

Brocks, J. J., & Summons, R. E. (2003). 8.03—Sedimentary Hydrocarbons, Biomarkers for Early Life. In H. D. Holland & K. K. Turekian (Eds.), *Treatise on Geochemistry* (pp. 63–115). Pergamon. https://doi.org/10.1016/B0-08-043751-6/08127-5

Campbell, I. H., & Allen, C. M. (2008). Formation of supercontinents linked to increases in atmospheric oxygen. *Nature Geoscience*, *1*(8), 554–558.

Cortial, F., Gauthier-Lafaye, F., Lacrampe-Couloume, G., Oberlin, A., & Weber, F. (1990). Characterization of organic matter associated with uranium deposits in the Francevillian

formation of Gabon (lower proterozoic). *Organic Geochemistry*, *15*(1), 73–85. https://doi.org/10.1016/0146-6380(90)90185-3

Court, R. W., Sephton, M. A., Parnell, J., & Gilmour, I. (2007). Raman spectroscopy of irradiated organic matter. *Geochimica et Cosmochimica Acta*, *71*(10), 2547–2568. https://doi.org/10.1016/j.gca.2007.03.001

Dutkiewicz, A., George, S. C., Mossman, D. J., Ridley, J., & Volk, H. (2007). Oil and its biomarkers associated with the Palaeoproterozoic Oklo natural fission reactors, Gabon. *Chemical Geology*, *244*(1), 130–154. https://doi.org/10.1016/j.chemgeo.2007.06.010

Duursma, E. K., & Boisson, M. (1994). Global oceanic and atmospheric oxygen stability considered in relation to the carbon-cycle and to different time scales. *Oceanologica Acta*, *17*(2), 117–141.

Ferralis, N., Matys, E. D., Knoll, A. H., Hallmann, C., & Summons, R. E. (2016). Rapid, direct and non-destructive assessment of fossil organic matter via microRaman spectroscopy. *Carbon*, *108*, 440–449. https://doi.org/10.1016/j.carbon.2016.07.039

Ferrari, A. C., & Basko, D. M. (2013). Raman spectroscopy as a versatile tool for studying the properties of graphene. *Nature Nanotechnology*, *8*(4), 235–246. https://doi.org/10.1038/nnano.2013.46

Fischer, W. W., Hemp, J., & Johnson, J. E. (2016). Evolution of oxygenic photosynthesis. *Annual Review of Earth and Planetary Sciences*, *44*(1), 647–683.

French, K. L., Hallmann, C., Hope, J. M., Schoon, P. L., Zumberge, J. A., Hoshino, Y., Peters, C. A., George, S. C., Love, G. D., Brocks, J. J., Buick, R., & Summons, R. E. (2015). Reappraisal of hydrocarbon biomarkers in Archean rocks. *Proceedings of the National Academy of Sciences*, *112*(19), 5915–5920. https://doi.org/10.1073/pnas.1419563112

Galimov, E. M., Girin, Y. P., & Vernadskiy, V. I. (1968). Variation in the isotopic composition of carbon during the formation of carbonate concretions. *Geochem. Int*, *5*, 178–182.

Gauthier-Lafaye, F., & Weber, F. (1989). The Francevillian (Lower Proterozoic) uranium ore deposits of Gabon. *Economic Geology*, *84*(8), 2267–2285. https://doi.org/10.2113/gsecongeo.84.8.2267

Gauthier-Lafaye, F., & Weber, F. (2003). Natural nuclear fission reactors: Time constraints for occurrence, and their relation to uranium and manganese deposits and to the evolution of

the atmosphere. *Precambrian Research*, *120*(1), 81–100. https://doi.org/10.1016/S0301-9268(02)00163-8

Gumsley, A. P., Chamberlain, K. R., Bleeker, W., Söderlund, U., De Kock, M. O., Larsson, E. R., & Bekker, A. (2017). Timing and tempo of the Great Oxidation Event. *Proceedings of the National Academy of Sciences*, *114*(8), 1811–1816.

Hallmann, C., French, K. L., & Brocks, J. J. (2022). Biomarkers in the Precambrian: Earth's ancient sedimentary record of life. *Elements*, *18*(2), 93–99.

Hayes, J. M., Strauss, H., & Kaufman, A. J. (1999). The abundance of 13C<math><msup><mi></mi><mn>13</mn></msup><mtext>C</mtext></math> in marine organic matter and isotopic fractionation in the global biogeochemical cycle of carbon during the past 800 Ma. *Chemical Geology*, *161*(1), 103–125. https://doi.org/10.1016/S0009-2541(99)00083-2

Hayes, J. M., & Waldbauer, J. R. (2006). The carbon cycle and associated redox processes through time. *Philosophical Transactions of the Royal Society B: Biological Sciences*, *361*(1470), 931–950. https://doi.org/10.1098/rstb.2006.1840

Henry, D. G., Jarvis, I., Gillmore, G., & Stephenson, M. (2019). Raman spectroscopy as a tool to determine the thermal maturity of organic matter: Application to sedimentary, metamorphic and structural geology. *Earth-Science Reviews*, *198*, 102936. https://doi.org/10.1016/j.earscirev.2019.102936

Hodgskiss, M. S., & Sperling, E. A. (2022). A prolonged, two-step oxygenation of Earth's early atmosphere: Support from confidence intervals. *Geology*, *50*(2), 158–162.

Holland, H. D. (2006). The oxygenation of the atmosphere and oceans. *Philosophical Transactions of the Royal Society B: Biological Sciences*, *361*(1470), 903–915.

Javaux, E. J., & Lepot, K. (2018). The Paleoproterozoic fossil record: Implications for the evolution of the biosphere during Earth's middle-age. *Earth-Science Reviews*, *176*, 68–86.

Kaneki, S., & Kouketsu, Y. (2022). An automatic peak deconvolution method for Raman spectra of terrestrial carbonaceous material for application to the geothermometers of Kouketsu et al., (2014). *Island Arc*, *31*(1), e12467. https://doi.org/10.1111/iar.12467

Karhu, J. A., & Holland, H. D. (1996). Carbon isotopes and the rise of atmospheric oxygen. *Geology*, *24*(10), 867–870.

Kouketsu, Y., Mizukami, T., Mori, H., Endo, S., Aoya, M., Hara, H., Nakamura, D., & Wallis, S. (2014). A new approach to develop the Raman carbonaceous material geothermometer for low-grade metamorphism using peak width. *Island Arc*, *23*(1), 33–50. https://doi.org/10.1111/iar.12057

Kump, L. R. (1991). Interpreting carbon-isotope excursions: Strangelove oceans. *Geology*, *19*(4), 299–302.

Laakso, T. A., & Schrag, D. P. (2022). The carbon isotope record and Earth surface oxygenation. *Isotopic Constraints on Earth System Processes*, 203–216.

Lecomte, A., Michels, R., Cathelineau, M., Morlot, C., Brouand, M., & Flotté, N. (2020). Uranium deposits of Franceville basin (Gabon): Role of organic matter and oil cracking on uranium mineralization. *Ore Geology Reviews*, *123*, 103579. https://doi.org/10.1016/j.oregeorev.2020.103579

Lekele Baghekema, S. G., Lepot, K., Riboulleau, A., Fadel, A., Trentesaux, A., & El Albani, A. (2017). Nanoscale analysis of preservation of ca. 2.1 Ga old Francevillian microfossils, Gabon. *Precambrian Research*, *301*, 1–18. https://doi.org/10.1016/j.precamres.2017.08.024

Lyons, T. W., Reinhard, C. T., & Planavsky, N. J. (2014). The rise of oxygen in Earth's early ocean and atmosphere. *Nature*, *506*(7488), 307–315. https://doi.org/10.1038/nature13068

Marais, D. J. D., Strauss, H., Summons, R. E., & Hayes, J. M. (1992). Carbon isotope evidence for the stepwise oxidation of the Proterozoic environment. *Nature*, *359*(6396), 605–609. https://doi.org/10.1038/359605a0

Martin, A. P., Condon, D. J., Prave, A. R., & Lepland, A. (2013). A review of temporal constraints for the Palaeoproterozoic large, positive carbonate carbon isotope excursion (the Lomagundi–Jatuli Event). *Earth-Science Reviews*, *127*, 242–261.

Mason, E., Edmonds, M., & Turchyn, A. V. (2017). Remobilization of crustal carbon may dominate volcanic arc emissions. *Science*, *357*(6348), 290–294. https://doi.org/10.1126/science.aan5049

Mathieu, R., Cuney, M., & Cathelineau, M. (2000). Geochemistry of palaeofluids circulation in the Franceville basin and around Oklo natural nuclear reaction zones (Gabon). *Journal of Geochemical Exploration*, *69–70*, 245–249. https://doi.org/10.1016/S0375-6742(00)00054-6

Mayika, K. B., Moussavou, M., Prave, A. R., Lepland, A., Mbina, M., & Kirsimäe, K. (2020). The Paleoproterozoic Francevillian succession of Gabon and the Lomagundi-Jatuli event. *Geology*, *48*(11), 1099–1104. https://doi.org/10.1130/G47651.1

Melezhik, V. A., Huhma, H., Condon, D. J., Fallick, A. E., & Whitehouse, M. J. (2007). Temporal constraints on the Paleoproterozoic Lomagundi-Jatuli carbon isotopic event. *Geology*, *35*(7), 655–658.

Mossman, D. J., Gauthier-Lafaye, F., & Jackson, S. E. (2001). Carbonaceous substances associated with the Paleoproterozoic natural nuclear fission reactors of Oklo, Gabon: Paragenesis, thermal maturation and carbon isotopic and trace element compositions. *Precambrian Research*, *106*(1), 135–148. https://doi.org/10.1016/S0301-9268(00)00129-7

Nagy, B., Leventhal, J. S., & Gauthier-Lafaye, F. (1991). Organic geochemical and petrological investigations of a natural reactor and its environs at Oklo, Gabon: A preliminary report. *US Geol Sury Circ*, *1058*, 65–67.

Ohmoto, H. (1996). Evidence in pre–2.2 Ga paleosols for the early evolution of atmospheric oxygen and terrestrial biota. *Geology*, *24*(12), 1135–1138. https://doi.org/10.1130/0091-7613(1996)024<1135:EIPGPF>2.3.CO;2

Ossa Ossa, F., El Albani, A., Hofmann, A., Bekker, A., Gauthier-Lafaye, F., Pambo, F., Meunier, A., Fontaine, C., Boulvais, P., Pierson-Wickmann, A.-C., Cavalazzi, B., & Macchiarelli, R. (2013). Exceptional preservation of expandable clay minerals in the ca. 2.1 Ga black shales of the Francevillian basin, Gabon and its implication for atmospheric oxygen accumulation. *Chemical Geology*, *362*, 181–192. https://doi.org/10.1016/j.chemgeo.2013.08.011

Ossa Ossa, F., Hofmann, A., Vidal, O., Kramers, J. D., Agangi, A., Belyanin, G. A., & Mayaga-Mikolo, F. (2014). Hydrothermal clay mineral formation in the uraniferous Paleoproterozoic FA Formation, Francevillian basin, Gabon. *Precambrian Research*, *246*, 134–149. https://doi.org/10.1016/j.precamres.2014.03.003

Planavsky, N. J., Bekker, A., Hofmann, A., Owens, J. D., & Lyons, T. W. (2012). Sulfur record of rising and falling marine oxygen and sulfate levels during the Lomagundi event. *Proceedings of the National Academy of Sciences*, *109*(45), 18300–18305. https://doi.org/10.1073/pnas.1120387109

Poulton, S. W., Bekker, A., Cumming, V. M., Zerkle, A. L., Canfield, D. E., & Johnston, D. T. (2021). A 200-million-year delay in permanent atmospheric oxygenation. *Nature*, *592*(7853), 232–236.

Rasmussen, B., Muhling, J. R., Tosca, N. J., & Fischer, W. W. (2023). Did nutrient-rich oceans fuel Earth's oxygenation? *Geology*, *51*(5), 444–448. https://doi.org/10.1130/G50835.1

Robbins, L. J., Fakhraee, M., Smith, A. J., Bishop, B. A., Swanner, E. D., Peacock, C. L., Wang, C.-L., Planavsky, N. J., Reinhard, C. T., & Crowe, S. A. (2023). Manganese oxides, Earth surface oxygenation, and the rise of oxygenic photosynthesis. *Earth-Science Reviews*, *239*, 104368.

Sánchez-Baracaldo, P. (2015). Origin of marine planktonic cyanobacteria. *Scientific Reports*, *5*(1), 17418.

Sánchez-Baracaldo, P., & Cardona, T. (2020). On the origin of oxygenic photosynthesis and Cyanobacteria. *New Phytologist*, *225*(4), 1440–1446.

Sánchez-Baracaldo, P., Raven, J. A., Pisani, D., & Knoll, A. H. (2017). Early photosynthetic eukaryotes inhabited low-salinity habitats. *Proceedings of the National Academy of Sciences*, *114*(37), E7737–E7745.

Sawaki, Y., Moussavou, M., Sato, T., Suzuki, K., Ligna, C., Asanuma, H., Sakata, S., Obayashi, H., Hirata, T., & Edou-Minko, A. (2017). Chronological constraints on the Paleoproterozoic Francevillian Group in Gabon. *Geoscience Frontiers*, *8*(2), 397–407. https://doi.org/10.1016/j.gsf.2016.10.001

Schidlowski, M. (1987). Application of stable carbon isotopes to early biochemical evolution on Earth. *Annual Review of Earth and Planetary Sciences, Vol. 15, p. 47*, *15*, 47.

Schidlowski, M., Eichmann, R., & Junge, C. E. (1975). Precambrian sedimentary carbonates: Carbon and oxygen isotope geochemistry and implications for the terrestrial oxygen budget. *Precambrian Research*, *2*(1), 1–69.

Schidlowski, M., Hayes, J. M., & Kaplan, I. R. (1983). *Isotopic inferences of ancient biochemistries-Carbon, sulfur, hydrogen, and nitrogen*.

Schmid, T., & Dariz, P. (2019). Raman Microspectroscopic Imaging of Binder Remnants in Historical Mortars Reveals Processing Conditions. *Heritage*, *2*(2), Article 2. https://doi.org/10.3390/heritage2020102

Shields, G., & Veizer, J. (2002). Precambrian marine carbonate isotope database: Version 1.1. *Geochemistry, Geophysics, Geosystems*, *3*(6), 1 of 12–12 12.

Smith, E., & Dent, G. (2004). Introduction, Basic Theory and Principles. In *Modern Raman Spectroscopy – A Practical Approach* (pp. 1–21). John Wiley & Sons, Ltd. https://doi.org/10.1002/0470011831.ch1

Strauss, H., & Beukes, N. J. (1996). Carbon and sulfur isotopic compositions of organic carbon and pyrite in sediments from the Transvaal Supergroup, South Africa. *Precambrian Research*, *79*(1–2), 57–71.

Summons, R. E., & Powell, T. G. (1986). Chlorobiaceae in Palaeozoic seas revealed by biological markers, isotopes and geology. *Nature*, *319*(6056), 763–765.

Thiéblemont, D., J.P., P., J.C., G., Gouin, J., M., T., Cocherie, A., C., G., Préat, A., Boulingui, B., H., E., & A.B, K. (2009). *Notice explicative de la Carte géologique de la République du Gabon à 1/200 000, feuille Fougamou. Editions DGMG – Ministères des Mines, du Pétrole, des Hydrocarbures. Libreville.*

Turner, P., Paton, K., Legge, E., de Luna Bugallo, A., Rocha-Robledo, A., Zahab, A.-A., Centeno, A., Sacco, A., Pesquera, A., Zurutuza, A., Rossi, A. M., Tran, D., L Silva, D., Losic, D., Farivar, F., Kerdoncuff, H., Kwon, H., Pirart, J., Campos, J. L. E., … Pollard, A. (2022). International interlaboratory comparison of Raman spectroscopic analysis of CVD-grown graphene. *2D Materials*, *9*(3), 035010. https://doi.org/10.1088/2053-1583/ac6cf3

Ward, L. M., Rasmussen, B., & Fischer, W. W. (2019). Primary productivity was limited by electron donors prior to the advent of oxygenic photosynthesis. *Journal of Geophysical Research: Biogeosciences*, *124*(2), 211–226.

Warke, M. R., Di Rocco, T., Zerkle, A. L., Lepland, A., Prave, A. R., Martin, A. P., Ueno, Y., Condon, D. J., & Claire, M. W. (2020). The great oxidation event preceded a paleoproterozoic "snowball Earth". *Proceedings of the National Academy of Sciences*, *117*(24), 13314–13320.

Weber, F. (1968). *Une série précambrienne du Gabon: Le Francevillien. Sédimentologie, géochimie, relations avec les gîtes minéraux associés* (Vol. 28, Issue 1). Persée-Portail des revues scientifiques en SHS.

Weber, F., & Gauthier-Lafaye, F. (2013). No proof from carbon isotopes in the Francevillian (Gabon) and Onega (Fennoscandian shield) basins of a global oxidation event at 1980-

2090 Ma following the Great Oxidation Event (GOE). *Comptes Rendus - Geoscience*, *345*(1), 28–35. https://doi.org/10.1016/j.crte.2012.12.003

Weber, F., Gauthier-Lafaye, F., Whitechurch, H., Ulrich, M., & El Albani, A. (2016). The 2-Ga Eburnean Orogeny in Gabon and the opening of the Francevillian intracratonic basins: A review. *Comptes Rendus Geoscience*, *348*(8), 572–586. https://doi.org/10.1016/j.crte.2016.07.003

Wogan, N. F., Catling, D. C., Zahnle, K. J., & Claire, M. W. (2022). Rapid timescale for an oxic transition during the Great Oxidation Event and the instability of low atmospheric O2. *Proceedings of the National Academy of Sciences*, *119*(37), e2205618119.

Yoshida, S., Mayika, K. B., Ishihara, Y., Moussavou, M., Asanuma, H., Sato, T., Hirata, T., Ligna, C., Sawaki, Y., & Edou-Minko, A. (2024). Depositional condition of Paleoproterozoic Francevillian carbonate rocks revisited from rare earth element contents. *Geoscience Frontiers*, *15*(3), 101771. https://doi.org/10.1016/j.gsf.2023.101771

Appendix 1

Table S1. Fitted Raman spectra peak parameters

Sample	Center D1	FWHM D1	Center D2	FWHM D2	Center G	FWHM G	Center D3	FWHM D3	Center D4	FWHM D4
9700-14	1338	122	1596	46	1581	119	1462	91	1245	182
AMD4	1331	87	1605	30	1598	88	1455	172	1245	145
AMD13	1330	93	1603	33	1593	73	1493	227	1245	153
AMD20	1331	94	1603	32	1595	72	1494	231	1245	153
AMD27	1328	82	1603	36	1571	70	1386	298	1245	148
AMD32	1334	97	1604	27	1596	67	1479	129	1245	140
AMD96,62	1334	93	1606	24	1600	60	1480	126	1245	133
BGB60	1329	85	1605	35	1590	86	1455	229	1245	169
BNFD1	1330	93	1605	28	1599	73	1473	139	1245	179
DM11	1341	92	1605	23	1596	48	1466	225	1245	138
DM34	1345	108	1600	38	1584	111	1466	88	1245	149
DM50	1341	103	1604	37	1590	59	1487	178	1245	129
DM174	1340	98	1602	27	1593	53	1484	188	1245	131
DM191	1339	95	1602	24	1594	55	1456	239	1245	154
FB35,5	1330	81	1605	32	1598	74	1467	263	1245	144
FB36,5	1333	95	1598	37	1595	87	1459	153	1245	108
FB46,2	1334	93	1605	31	1596	66	1477	120	1245	134
LST12-31,3_1	1340	100	1597	30	1595	53	1483	176	1245	136
LST12-31,3_2	1339	99	1601	38	1589	52	1476	223	1245	157
LST12-35,45	1339	94	1602	37	1588	50	1475	219	1245	150
LST12-54,25	1340	98	1603	39	1589	52	1475	227	1245	159
LST12-55,66	1340	100	1617	12	1598	44	1485	203	1245	152
LST12-61,18	1339	88	1610	35	1596	46	1485	215	1245	154
LST12-78,7	1337	97	1602	26	1597	52	1486	216	1245	136
ML594-4	1329	89	1606	35	1594	90	1452	181	1245	170
ML594-14	1328	86	1604	35	1595	79	1462	269	1245	163
ML594-17	1325	86	1604	36	1590	90	1434	224	1245	177
ML605-3	1327	84	1605	39	1584	115	1422	168	1245	159
ML605-10	1329	86	1605	34	1597	70	1638	98	1245	135
ML605-16	1327	86	1604	39	1587	100	1426	256	1245	175
ML605-21	1326	82	1605	42	1552	123	1398	154	1245	167
ML605-26	1327	87	1605	38	1590	96	1444	185	1245	171
ML605-37	1328	86	1603	33	1595	76	1464	256	1245	149
MLD-24-02	1326	82	1604	35	1593	94	1440	195	1245	162
MLD-24-41	1331	120	1605	44	1588	72	1493	174	1245	159
MLD-24-58	1327	91	1607	31	1599	63	1479	199	1245	171

Lihtlitsents lõputöö reprodutseerimiseks ja üldsusele kättesaadavaks tegemiseks

Mina, Georg Rahu,

1. annan Tartu Ülikoolile tasuta loa (lihtlitsentsi) minu loodud teose

Raman spectroscopy study of the sedimentary organic material thermal alteration in the Paleoproterozoic Francevillian Basin, Gabon

mille juhendajad on Kalle Kirsimäe ja Tavo Romann

reprodutseerimiseks eesmärgiga seda säilitada, sealhulgas lisada digitaalarhiivi DSpace kuni autoriõiguse kehtivuse lõppemiseni.

2. Annan Tartu Ülikoolile loa teha punktis 1 nimetatud teos üldsusele kättesaadavaks Tartu Ülikooli veebikeskkonna, sealhulgas digitaalarhiivi DSpace kaudu Creative Commonsi litsentsiga CC BY NC ND 4.0, mis lubab autorile viidates teost reprodutseerida, levitada ja üldsusele suunata ning keelab luua tuletatud teost ja kasutada teost ärieesmärgil, kuni autoriõiguse kehtivuse lõppemiseni.

3. Olen teadlik, et punktides 1 ja 2 nimetatud õigused jäävad alles ka autorile.

4. Kinnitan, et lihtlitsentsi andmisega ei riku ma teiste isikute intellektuaalomandi ega isikuandmete kaitse õigusaktidest tulenevaid õigusi.

Georg Rahu

25.05.2025